Journal of Cleaner Production 469 (2024) 143254

Contents lists available at ScienceDirect

Journal of Cleaner Production

journal homepage: www.elsevier.com/locate/jclepro

Exploring the role of hydrogen in decarbonizing energy-intensive industries: A techno-economic analysis of a solid oxide fuel cell cogeneration system

A. Ademollo [a,*], A. Mati [a], M. Pagliai [b], C. Carcasci [a]

[a] *Università degli Studi di Firenze, Department of Industrial Engineering - DIEF, Via di Santa Marta 3, 50139, Firenze, Italy*
[b] *Università degli Studi di Firenze, Department of Chemistry 'Ugo Schiff' – DICUS Via della Lastruccia 3, 50019 Sesto Fiorentino, Italy*

ARTICLE INFO

Handling Editor: Kathleen Aviso

Keywords:
Solid oxide fuel cell
Power to hydrogen
Levelized cost of hydrogen
Net present costs
Energy intensive industry

ABSTRACT

Industry is nowadays one of the most energy-demanding sectors representing a major contributor of global greenhouse gas emissions. The simultaneous need for electricity and high-temperature heat is what makes some industrial processes difficult to decarbonize via current commercially available technologies. As the demand for materials and goods is expected to grow in the upcoming years, it is crucial to define which strategies and technologies will serve as the cornerstone of sustainable development. This study addresses the imperative need for emission reduction of energy-intensive sectors by proposing a novel hydrogen-based cogeneration system in the framework of the paper and pulp industry, with the aim of providing general insights relevant to a broader spectrum of similar applications. The comparative analysis presented in this work focuses on three cogeneration options aimed at satisfying the paper mill energy needs: a conventional natural gas-fuelled gas turbine, a Solid Oxide Fuel Cell (SOFC) fed with grey hydrogen produced via steam methane reforming, and a SOFC operating using green hydrogen produced on-site. The latter involves an integrated multi-energy system with photovoltaic panels, electrolyzers, compressors, and storage tanks. Indeed, the SOFC potential of supplying electricity and high-temperature heat in the form of pressurized steam for industrial applications has not been well investigated yet and represents one of the main objectives of this work. Building on the real consumption profiles of a paper mill facility, techno-economic analyses are carried out for many system configurations, varying components size and layout to assess their performance with respect to CO_2 emissions and two key economic parameters, the Levelized Cost of Hydrogen (LCOH) and the net present cost. An in-house-developed flexible simulation framework is presented and expanded for the purposes of this study, including a detailed model that accounts for design and off-design performance of a SOFC cogeneration unit. Results demonstrate that integrating a SOFC with a heat recovery steam generator result in a 75% reduction in the mass flow of generable pressurized steam in comparison to a gas turbine. Additionally, in the cost-optimal scenario, CO_2 emissions are 25% lower than the conventional gas turbine-based configuration, achieving complete independence from the electricity grid and an LCOH of 5.81€/kg without considering revenues from electricity sold.

1. Introduction

The upgrading of existing energy systems with an ever-increasing share of renewable energy sources is crucial to reduce greenhouse gases into the atmosphere. Furthermore, the European Commission, both through the introduction in 2019 of the European Green Deal (European Commission, 2019) and also with the more recent approval of the REPowerEU plan (European Commission, 2022), sets several targets for 2030 and 2050 aimed at decarbonization and the achievement of energy independence.

In this scenario, the advancement of the energy system will be of primary importance, encompassing the adoption of multiple energy carriers towards a greater level of integration, thus leading to the coupling of electricity and Natural Gas (NG) with sustainable fuels such as biofuels and renewable hydrogen (Ademollo et al., 2023; Farfan et al., 2019; Genovese et al., 2023). In this context, industry, characterized by

* Corresponding author.
E-mail addresses: andrea.ademollo@unifi.it (A. Ademollo), alessandro.mati@unifi.it (A. Mati), marco.pagliai@unifi.it (M. Pagliai), carlo.carcasci@unifi.it (C. Carcasci).

https://doi.org/10.1016/j.jclepro.2024.143254
Received 17 April 2024; Received in revised form 22 July 2024; Accepted 23 July 2024
Available online 24 July 2024

energy-intensive operations in plants such as foundries, cement factories, steelmaking, and papermills, stands out as one of the highest energy-consuming sectors of the economy. Several studies have dealt with the analysis of industrial applications where the high level of energy consumption is inherently related to the nature of the process. The area of focus ranges from plastic manufacturing (Dunkelberg et al., 2018) and glass (Griffin et al., 2021) up to ceramics and steel production (Ding et al., 2023). The replacement of conventional fossil fuels with sustainable energy carriers in the steel industry is a promising route towards emissions abatement (Meng et al., 2024; Salimbeni et al., 2023; Superchi et al., 2023).

Among the industrial processes with potential for process integration and efficiency improvement, the pulp and paper sector accounts for about 5% of the world's total industrial final energy consumption and reports 2% of the sector's direct CO_2 emissions (Global Efficiency Intelligence, 2023; IEA, 2023). Due to its process nature, the pulp and paper industry is characterized by simultaneous high electricity and heat consumption, which means it is well suited for the adoption of cogeneration. Several types of power systems can be employed as Combined Heat and Power (CHP) plants for this purpose, as presented in Ref. (Shabbir and Mirzaeian, 2016) like internal combustion engines, gas turbines, steam turbines, and combined cycles. In this context, Gas Turbine (GT) based CHP systems present a long record in literature and are widely adopted for this type of applications due to their proven energy efficiency. Nevertheless, increasing energy efficiency alone might not cope with decarbonization targets, and it is necessary to design innovative solutions enabling high penetration of renewable energy. Hydrogen represents a promising alternative for these applications where direct electrification is not possible and its versatility makes it a favorable energy carrier, as it can be rapidly converted into mechanical, thermal, and electrical energy using internal combustion engines, GTs, steam engines, and fuel cells (Burton et al., 2021). Accordingly, Solid Oxide Fuel Cells (SOFC) potential for industrial-scale applications is investigated in this study as a viable option to GTs, mainly because of high efficiencies and reduced environmental footprint (Singh et al., 2021). To the best of the author's knowledge, this concept has not been extensively studied in previous research, and there is ample scope for further exploration considering the integration of renewable hydrogen in the framework of multi-energy systems.

1.1. Fuel cells cogeneration in integrated energy systems

The SOFC cogeneration concept is widely discussed in the literature, and commercial products have already entered the market. Nevertheless, most cases have focused on the residential sector, mostly for the supply of hot water at low temperatures (below 100 °C) (Arsalis, 2019; Mottaghizadeh et al., 2022). Fuel cells suitable for cogeneration applications are those operating in a temperature range between 600 °C and 1000 °C. These include SOFCs, Molten Carbonate Fuel Cells (MCFCs) and Direct Carbon Fuel Cells (DCFCs). Compared to the other FC technologies, as of today, SOFCs turn out to be the best available for the following reasons (Cigolotti et al., 2021; Ozalp et al., 2022).

- Faster system start-up and response time.
- Wide range of applicability: from residential scale (kW_{el}) to industrial scale (MW_{el}).
- Good compromise between cost and efficiency, both thermal and electrical.
- High operating temperatures: optimum for cogeneration
- Higher technology readiness level than DCFC.
- Lower costs per kW_{el} than MCFCs.

Previous research has focused on understanding the influence of different system's configurations and key parameters on SOFC cogeneration performance (Pirkandi et al., 2012; Zhou et al., 2022). Singh et al. provided an exhaustive compendium on SOFCs, highlighting positive traits such as compactness and high electrical efficiency, underlining the important challenges for an ever-widening market penetration (Singh et al., 2021). Aligned with the technology development, a shift toward industrial applications seems inevitable. The traditional approach for SOFC cogeneration consists in the recovery of the residual heat usually not exceeding 200 °C, thus restricting its area of application (Shi et al., 2019), while on the other hand, industrial demand often goes beyond this threshold, often requiring heat in the form of steam, as it is the case for the paper industry. Zhao et al. have proposed a new layout for a SOFC cogeneration system to produce high-temperature steam for industrial applications (Zhao et al., 2023). They explore the influence of different gas split locations on the system performance to produce steam at medium, low and super low pressures.

The aim of this study is to extend the analysis to a wider framework, where the performance of traditional and SOFC cogeneration solutions is explored in a multi-energy system scenario interacting with the variable demand of a paper mill facility. Matching demanding energy needs with environmentally-friendly fuels is an increasingly pressing challenge and this is where green hydrogen is expected to play a relevant role. With respect to this aspect, Vialetto et al. have proposed an analysis focusing on the integration of a reversible Solid Oxide cell (rSOC) system into a paper mill's cogeneration system, where additional hydrogen production is also included (Vialetto et al., 2019). In another study, Posdziech et al. conducted a study over different large-scale prototype applications of rSOC technology, including hydrogen-based energy storage, integration into a steel plant, and coupling with a pressurized Solid Oxide Electrolysis Cell (SOEC) and methanation unit (Posdziech et al., 2019).

1.2. Aims of the study and novelty

Techno-economic analyses of proposed solutions are needed to assess the feasibility of projects on a commercial scale while also defining their environmental impact via key performance indicators. Comprehensive analyses in this field have been conducted in the steel sector (Superchi et al., 2023; Marocco et al., 2024), and following a similar approach, a groundwork for this study by some of the authors has addressed the adoption of a hydrogen-fuelled GT cogeneration system in a paper mill facility (Mati et al., 2023).

Building on methods and insights from the up-to-date research, the current analysis intends to move further exploring the techno-economic feasibility of a SOFC cogeneration system fed with renewable hydrogen to provide high-temperature heat and electricity for industrial purposes. While decarbonization of paper industry is extensively explored in the literature, there is lack of studies assessing the SOFC potential for supplying high-temperature heat as an alternative to traditional fossil fuel-based solutions. If on the one hand renewable energy can be easily integrated to satisfy the electricity demand, direct electrification of heat supply poses some challenges due to the demanding heat properties required by the process nature. This gap not only highlights how difficult it is to replace traditional heat production with direct electrification, but it also lays the groundwork for this study to analyze the SOFC systems capacity to efficiently convert renewable energy (in the form of hydrogen) into high-temperature heat and electricity, thereby reducing the carbon footprint of one of the most energy-intensive sectors.

Thus, leveraging on the real electrical and thermal demand profiles of a paper mill, this work proposes a novel SOFC cogeneration system integrated into a broader multi-energy scenario that incorporates renewables and the hydrogen value chain. The main goal is to conduct a comprehensive techno-economic assessment yielding insights into the potential of this solution discussed in comparison with more traditional options. A dedicated simulation framework is developed and simulations are carried out based on an hourly temporal resolution, accounting for an accurate modelling of partial-load performance of the main components to evaluate cost-optimal and environmentally effective solutions. To the best of the author's knowledge this type of analysis has

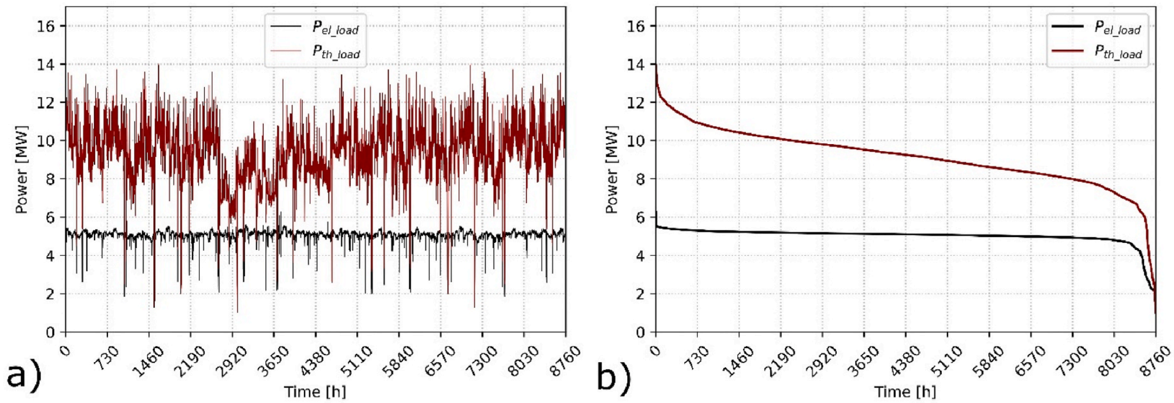

Fig. 1. a) Electric and thermal load profiles. b) Electric and thermal load curve.

not yet been conducted for the technology under evaluation at the proposed level of detail.

This study extends beyond the current body of knowledge in several ways.

a. It assesses the hydrogen decarbonization potential for industrial-scale SOFC-based cogeneration applications, encompassing all the major aspects of production, storage and conversion by means of innovative technologies. Environmental and economic impacts of hydrogen integration both as a sustainable fuel and as an energy storage medium are quantified.
b. It explores the utilization of a dedicated simulation framework that accounts for an accurate modelling of partial-load performance of main components establishing a reliable and replicable methodology for this kind of applications.
c. The study analyses the novel configuration with respect to conventional systems, including Gas Turbine (GT) configuration and SOFC fuelled with grey hydrogen from Steam Methane Reformer (SMR), thus benchmarking the environmental and economic advantages of integrating renewable hydrogen into industrial cogeneration systems.
d. A key feature is the detailed modelling of heat transfer processes for high-temperature steam production in both SOFC and GT systems. This involves rigorously considering the composition and characteristics of exhaust flows, and key thermodynamic parameters in the Heat Recovery Steam Generator (HRSG) process to effectively assess thermal output power convertible into pressurized steam improving the accuracy of the analysis. The prospect for the industrial exploitation of high-temperature thermal byproduct from SOFC technology is presented accordingly.
e. By combining simulation-based optimization and sensitivity analyses over system components capacities and energy prices, it introduces a comprehensive assessment of critical economic indicators such as the Levelized Cost of Hydrogen (LCOH) and the Net Present Costs (NPC). This approach provides a nuanced understanding of the techno-economic benefits of using hydrogen in CHP systems under different energy market conditions, thereby presenting up-to-date methods for advancing the optimization of innovative multi-energy systems.

Insights into the emissions reduction potential of the proposed solutions have broad applicability in highly industrialized countries, where significant decarbonization opportunities remain untapped, serving as a viable route to achieving substantial reductions in industrial carbon footprints globally.

To address the presented aims, the paper has been organized as follows. First, Section 2. describes the modelling framework developed for the analysis and the thermodynamic models of the different technologies considered in system. A special focus is dedicated to the modelling and validation of SOFC component intended for cogeneration purposes. The case study is then presented in Section 2.4, where the description of the plant architecture, the SOFC and GT performance and coupling with the HRSG and the operating logic of the plant is provided. The main economic assumptions and parameters are also presented in this section. Section 3. outlines the main results of the energy balance analysis, as well as the economic one, identifying the optimal configuration definition based on the results derived from the CHP system simulation. Finally, in Section 4. , main conclusions are outlined.

Table 1
Key data characteristics.

	P_{el_load} [MW_{el}]	P_{th_load} [MW_{th}]
Maximum	6.28	13.95
Minimum	1.84	1.01
Mean	5.01	9.14
¼ (2190 h)	4.98	8.33
¾ (6570 h)	5.19	10.07
Max area rectangle	4.69	7.74
Standard deviation	0.45	1.50

2. Materials and methods

In this section, a concise overview of data analysis is initially conducted, followed by the modelling and validation of the SOFC, as well as the modelling of the auxiliary plant components and the case study investigation.

2.1. Data analysis

The considered case study focuses on a paper mill plant in Tuscany (Italy), with electricity and thermal consumption data provided for one year of operations. The heat demand is represented by saturated steam at a constant pressure of 20 bar for the process needs. As a baseline-scenario overall energy demand is covered for the most part by a traditional GT CHP system fuelled with NG. The cogeneration system consists of a GT which produces electricity that directly supply the facility request. The exhaust gases from the turbine are then directed to a Heat Recovery Steam Generator (HRSG) which recovers the thermal energy necessary to produce the required process steam. The feasibility of converting the CHP system to run on locally produced green hydrogen through a SOFC, via designing an optimized production and storage system combination, is evaluated in this study from both a technological and economic perspective.

Fig. 1 represents both demands as load profiles and as cumulative curves throughout the year.

From these figures it is highlighted how electrical consumption is relatively stable throughout the year, while the thermal one is higher and characterized by greater fluctuations.

A brief analysis of the data allows for the identification of key characteristics of the resulting curves, that are listed in Table 1.

2.2. Energy system modelling

2.2.1. Solid oxide fuel cell

A Solid Oxide Fuel Cell (SOFC) is an electrochemical device that allows the conversion of chemical energy in electric energy and heat, usually through the chemical reaction reported in eq. (1) (Singh et al., 2021):

$$H_{2(g)} + \frac{1}{2}O_{2(g)} = H_2O_{(g)} \tag{1}$$

At the cathode there is formation of the O^{2-} ion, which is transported to the anode through the electrolyte. The low ionic conductivity of the electrolyte, as well as the reduced electrochemical activity of the cathode, imposes the SOFC to work in a temperature range between 800 °C and 1000 °C (Wang et al., 2020), thus allowing the H_2 internal reforming and the heating of the incoming species without using a catalyst.

To characterize the operation of the SOFC, it is necessary to determine the polarization curve. O'Hayre et al. (O'Hayre, 2016) express the single cell potential as a function of current density as stated in eq. (2):

$$V_{cell} = \left(E_{0,cell} - \Delta V_{act} - \Delta V_{ohm} - \Delta V_{conc}\right) = f(i_{cell}) \tag{2}$$

Where $E_{0,cell}$, ΔV_{act}, ΔV_{ohm}, ΔV_{conc} and i_{cell} are respectively the open circuit potential, the activation overvoltage, the ohmic overvoltage, the concentration overvoltage and the current density circulating in the cell.

The open circuit potential is the maximum reachable voltage value for the open circuit and corresponds to 1.16 V, as it can be calculated by the Nernst equation (eq. (3)).

$$E_{0,cell} = E_0 + \frac{\Delta s_0}{2F} \times (T_{cell} - T_0) - \frac{R \times T_{cell}}{2F} \times ln\left(\frac{Pr_{H2} \times Pr_{O2}^{0.5}}{Pr_{H2O}}\right) \tag{3}$$

Where E_0, Δs_0, F, T_{cell}, T_0, R, Pr_{H2}, Pr_{O2} and Pr_{H2O} are, respectively, the standard reduction potential, the entropy of formation under standard conditions (15 °C and 1 atm), Faraday's constant, the working temperature of the cell, the standard temperature, the universal gas constant, the inlet pressure of H_2, the inlet pressure of O_2 in the air, and the outlet pressure of H_2O (equal to 1 atm).

As shown by O'Hayre et al. (O'Hayre, 2016) the ΔV_{ohm} term is expressed by eq. (4).

$$\Delta V_{ohm} = i \times ASR = i \times \frac{t_{elec}}{\sigma_{elec}} = i \times \frac{t_{elec} \times T_{cell}}{k \times exp^{-\frac{\Delta G_{act}}{(RT)}}} \tag{4}$$

Where ASR, t_{elec}, σ_{elec}, k and ΔG_{act} are respectively the area specific resistance and the electrolyte thickness, conductivity, specific constant (equal to 9000 K/Ωm), and activation energy.

Activation and concentration losses are evaluated within eq. (5), as reported in (O'Hayre, 2016). The anodic contribution to concentration losses is neglected as it is lower than the cathodic one.

$$\Delta V_{conc} = \frac{R \times T_{cell}}{4F \times \alpha} \times ln\left\{\frac{i}{i_{0,c} \times \left[x_{O_2} - \frac{t_c \times i \times R \times T_{cell}}{\left(4F \times Pr_{air,c} \times D^{eff}_{O_2,N_2}\right)}\right]}\right\} \tag{5}$$

Where α, $i_{0,c}$, x_{O_2}, t_c, $Pr_{air,c}$ and $D^{eff}_{O_2,N_2}$ are respectively the transfer coefficient (usually equal to 0.5), the cathode exchange current density, the O_2 molar fraction (equal to 0.21), the cathode thickness (equal to 0.8 mm), the operating air pressure at the cathode and the effective O_2 diffusivity coefficient (equal to 0.2 cm^2/s).

The cathode exchange current density is calculated as in eq. (6):

$$i_{0,c} = i^0_{0,c} \times exp^{\left(\frac{b_{act} \times J_{0,c}}{R}\right) \times \left(\frac{1}{T_{ref}} - \frac{1}{T_{cell}}\right)} \tag{6}$$

Where $i^0_{0,c}$, $J_{0,c}$, b_{act} and T_{ref} are respectively the cathode exchange current density at reference, the cathode activation energy, the activation coefficient (equal to 10) and the reference temperature (equal to 750 °C).

Thus, once the polarization curve is known, the SOFC active area (A_{SOFC}) is calculated as in eq. (7):

$$A_{SOFC} = \frac{P_{nom}}{V_{cell,min} \times N_{cell} \times i_{max}} \tag{7}$$

Where N_{cell} is the number of cells and P_{nom} is the nominal power of the SOFC, i.e., the one corresponding to the minimum fuel cell voltage and its maximum current density.

The H_2 mass flow rate required for the reaction to occur is obtained by eq. (8), (Wang et al., 2012):

$$\dot{m}_{H_2,in} = \frac{I_{cell} \times M_{H_2} \times N_{cell}}{F} \tag{8}$$

Where I_{cell} and M_{H_2} are respectively the current produced by the fuel cell and the H_2 molar mass.

The requested air flow rate is calculated as in eq. (9).

$$\dot{m}_{air,in} = \frac{M_{air} \times P_{req} \times N_{cell}}{2F \times V_{stack}} \times \lambda \tag{9}$$

Where M_{air}, P_{req}, V_{stack} and λ are respectively the air molar mass, the required output power, the stack voltage, and a stoichiometric coefficient (usually equal to 2) to consider the stack as working under excess air conditions.

The air outlet mass flow rate is calculated as in eq. (10).

$$\dot{m}_{air,out} = \dot{m}_{air,in} - x_{O_2} \times \dot{m}_{air,in} \tag{10}$$

The water vapor outlet mass flow rate is calculated as in eq. (11).

$$\dot{m}_{H_2O,out} = \dot{m}_{H_2,in} + \frac{x_{O_2} \times \dot{m}_{air,in}}{2} \tag{11}$$

Finally, the heat generated by the SOFC is calculated as in eq. (12).

$$Q_{SOFC} = \left(z \times T_{cell} \times \Delta_s + I_{cell} \times \sum \Delta V_i\right) \times N_{cell} \tag{12}$$

Where ΔV_i are the various contributions of activation, ohmic and concentration losses while z and Δ_s are respectively the molar flow rate and the entropy change, defined as in eqs. (13) and (14).

$$z = I_{cell} \times (2F)^{-1} \tag{13}$$

$$\Delta_s = -\left[\left(s^0_{H_2O} - s^0_{H_2} - \frac{1}{2}s^0_{O_2}\right) + \frac{R}{2} \times ln\left(\frac{P^2_{H_2} \times P_{O_2}}{P^2_{H_2O}}\right)\right] \tag{14}$$

Given that reactant temperature must be raised to the design value for the reaction to take place, it is important to account for the energy spent during the heating of the incoming air and H_2 streams. Ramp-up operations of the SOFC have orders of magnitude of hours, during which externally sourced heat must be supplied. One of the most active fields of research on SOFCs is related to the reduction of start-up times. In fact, several studies are reported in the literature regarding the reduction of times for start-up to less than 10 min (Bossel, 2012; Singh et al., 2021; Tucker, 2010). However, commercial solutions with start-up times of about or less than 1 h already exist, such as those offered, for example, by RedHawk Energy Systems (RedHawk Energy,

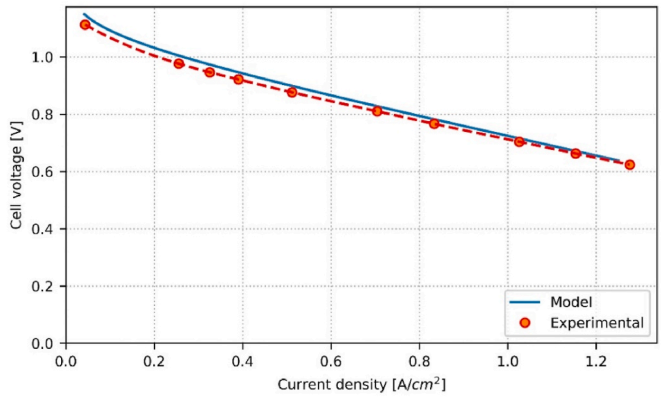

Fig. 2. SOFC model validation.

Table 2
SOFC design parameters.

Single module design parameters	Symbol	Value	Unit	Ref
Nominal power	P_{nom}	100	kW	
Electric efficiency	$\eta_{el,SOFC}$	50.5	%	
SOFC area	A_{SOFC}	1292	cm^2	
Number of cells	N_{cell}	97	–	
Current density range	Range i_{cell}	0.041 ÷ 1.25	A/cm^2	O'Hayre (2016)
Inlet H_2 pressure	$Pr_{H2,in}$	116000	Pa	Shin et al. (2021)
Inlet air pressure	$Pr_{air,in}$	101325	Pa	Shin et al. (2021)
Operating temperature	T_{des}	800	°C	O'Hayre (2016)
Exchange cathode current density at reference	$i^0_{0,c}$	0.2	A/cm^2	(O'Hayre, 2016; Shin et al., 2021)
Cathode activation energy	$J_{0,c}$	160	kJ/mol	Ahmadi et al. (2017)
Electrolyte thickness	t_{elec}	0.03	mm	O'Hayre (2016)

2023) or GenCell (2023). Once steady conditions are reached, then, the high operating temperature allows air and H_2 to be heated directly in the anode and cathode channels by the electrochemical process itself. As a result, the exploitable heat available for cogeneration purposes is calculated by subtracting from the total heat the fraction required to heat the mass of air and H_2 entering the cell, as expressed in eq. (15).

$$Q_{net} = Q_{SOFC} - \dot{m}_{air,in} \times c_{p,air} \times (T_{cell} - T_{amb}) - \dot{m}_{H_2,in} \times c_{p,H_2} \times (T_{cell} - T_{H_2}) \tag{15}$$

Where T_{H_2} is the H_2 temperature in the tank.

The electrical efficiency of the process stack is calculated by dividing the stack voltage by the product of the open-circuit potential and the number of cells as presented in eq. (16).

$$\eta_{el,stack} = \frac{V_{stack}}{E_{0,cell} \times N_{cell}} \tag{16}$$

The stack thermal efficiency is expressed by eq. (17).

$$\eta_{th,stack} = -\frac{\Delta G}{HHV_{H_{2,mol}}} \tag{17}$$

Where ΔG represents the Gibbs free energy at working conditions and is defined by eq. (18).

$$\Delta G = \Delta G^0 - \frac{R \times T_{cell}}{2F} \times ln\left(\frac{Pr_{H_2} \times Pr_{O_2}^{\frac{1}{2}}}{Pr_{H_2O}}\right) \tag{18}$$

Where ΔG^0 represents the Gibbs free energy at standard conditions.

Finally, the electrochemical efficiency of the stack is obtained as the product between electrical and thermal efficiencies as in eq. (19).

$$\eta_{SOFC} = \eta_{el,stack} \times \eta_{th} \tag{19}$$

Electrical and thermal efficiency of the system are related to hydrogen Lower Heating Value (LHV). The electrical efficiency is calculated by relating the electric power to the input hydrogen chemical power as in eq. (20).

$$\eta_{el} = \frac{P_{nom}}{\dot{m}_{H_2} \times LHV_{H_2}} \tag{20}$$

The thermal efficiency of the system composed by the SOFC and the Heat Recovery Steam Generator (HRSG) is determined by the ratio of the power generated in the form of saturated steam to the input chemical power of the hydrogen fuel as in eq. (21).

$$\eta_{th} = \frac{\dot{m}_{st} \times h_{st}}{\dot{m}_{H_2} \times LHV_{H_2}} \tag{21}$$

Where h_{st} is the enthalpy of saturated steam.

The total efficiency of the system is the sum of the electrical efficiency and the thermal efficiency as in eq. (22).

$$\eta_{tot} = \eta_{el} + \eta_{th} \tag{22}$$

2.2.2. SOFC validation

With respect to the SOFC model, the polarization curve is computed as the most representative characteristic of the fuel cell behavior. Spanning over a predefined range of current density values (whose extremes are represented by i_{min} and i_{max}), voltage of the cell is calculated backwards according to the presented set of equations and input parameters.

The modeling results are validated with experimental data for a single cell from the work of O'Hayre et al. (O'Hayre, 2016) comparing the different i-V curves.

The findings of the model display strong agreement with the data, as

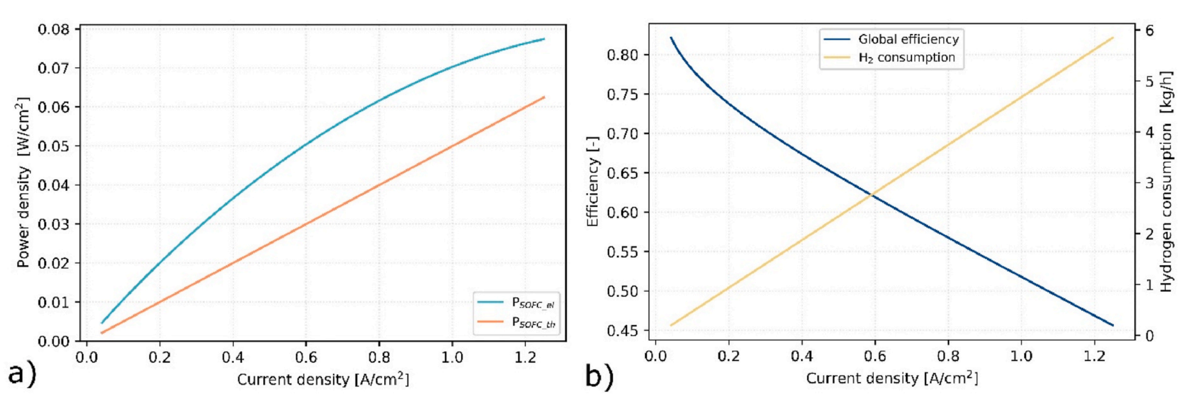

Fig. 3. a) Power density b) SOFC global efficiency and H_2 consumption.

shown in Fig. 2 and have a high coefficient of determination (R^2) value of 0.9892. Such validation has provided a solid foundation for further development towards the characterization of the technology's performance presented in Fig. 3.

The plots displayed in Fig. 3 are representative of the main performance characteristics for the SOFC single cell considering as input the design parameters listed in Table 2.

A module of 100 kW rated power has been considered representative for the targeted industrial-scale application. Deriving from the main thermodynamic limits and further assumptions for the technology based on the literature review, the geometry and the number of cells operating in the single stack is defined. The model is then provided with the design pressure and temperature values specified for the electrochemical reaction to run numerical simulation determining its main operational performance. It can be noticed that the electric power density of the single cells increases with increasing current density up to a maximum value of 0.078 W/cm^2 obtained for 1.25 A/cm^2, while at the same time thermal power density and hydrogen consumption both grow according to a linear trend. Since higher current values lead to a gradual decrease in the available electric power, with a significant reduction in the fuel cell efficiency caused by increased losses, the maximum operating current density value was set equal to the one defining the maximum power output. The curve's decreasing behavior after the maximum can be attributed to the increase in losses. Beyond a certain current value, the losses cause an increasingly greater voltage drop and, consequently, a decrease in the electric power produced, as it can be seen from both the polarization and efficiency curves.

Building on the design performance curves defined earlier, the modeling of the case study implemented multiple 100 kW-rated power modules operating in series, whose activation and cumulative performance are closely dependent on the load required at each timestep by the paper mill, as described in more detail in the specific section.

To transform the thermal energy generated by the SOFC into saturated steam at a constant pressure of 20 bar, the exhaust gases, primarily consisting of air (devoid of oxygen due to its consumption in the electrochemical reaction) and water vapor, pass through the HRSG section. During this process, heat is exchanged with the water-steam circuit, allowing for a precise evaluation of the facility's thermal load satisfaction throughout each considered time period.

2.2.3. *Solar energy*

To accurately estimate the producibility of green hydrogen in one year of operation, solar energy production potential for the selected location has been retrieved from the Photovoltaic Geographical Information System (PVGIS) database (European Commission, 2023) with an hourly resolution. Such a database provides data derived from long-term measurements, organized according to the typical meteorological year methodology which represent a statistically 'typical' year that incorporates variations in solar radiation, temperature and other relevant weather parameters serving as a reference for predicting solar energy production at a specific location. Normalized production data are then scaled according to the considered PV field size. The reference year used for the simulations is 2015.

2.2.4. *Electrolyzer*

For the considered case study Proton Exchange Membrane (PEM) Electrolyzers (EL) have been considered to assess the hydrogen production capabilities. The reasons behind this choice are the advantageous features of rapid response to PV power generation, high product purity and a good compromise between cost, efficiency, high current density, and low operating temperatures (Ju et al., 2018; Nikolaidis and Poullikkas, 2017). A detailed model of a PEM electrolyzer has been developed by the authors in previous works and it is described in ref. (Lubello et al., 2022; Mati et al., 2023). The modelled EL consists of modules of 200 kW rated power, characterized by an efficiency equal to 0.655, corresponding to an electric efficiency equal to 4.55 kWh/Nm3.

2.2.5. *Compressor*

A compression system is needed for on-site production in order to pressurize hydrogen from the electrolyze outlet pressure (30 bar) to 300 bar which is the value at which it is stored. Power consumption is estimated from an adiabatic compression model with an efficiency of 50%. This efficiency considers the efficiency of electrical power transformation and auxiliary systems such as the cooling circuit as assessed by the final report of Tractebel, Engie and Hinicio (Tractebel et al., 2017)

2.2.6. *Hydrogen storage system*

It is crucial to consider a daily storage system (as assessed by Moran in ref (Moran et al., 2023).) to store green hydrogen produced during PV surplus periods for SOFC operation during the night. In fact, a seasonal storage would incur significantly higher costs. It is worth noting that the paper mill demand must be met even during night-time hours when renewable production is unavailable, which calls for an increase in storage system capacity compared to continuous electrolyzer operation. The produced hydrogen is stored in tanks at a pressure of 300 bar, matching the compressor's outlet pressure. The storage system's State of Charge (SOC) is dynamically updated at each time step by the model, balancing hydrogen production and demand. This allows the stored hydrogen level to initially fluctuate between positive and negative values throughout the simulation year, before aligning the minimum with a SOC of 0%.

2.2.7. *Steam Methane Reformer*

The standard steam methane reforming process utilizes methane as the feedstock. Preheated and pressurized methane is combined with steam and fed into the reformer, where it transforms methane and steam into syngas. The resulting syngas undergoes cooling before entering high-temperature and low-temperature water-gas shift reactors in series. The shifted synthesis gas is further cooled for water condensation and processed for CO_2 removal and then a pressure swing adsorption system is employed to generate purified H_2 at temperatures of approximately 35–40 °C and 99.9% purity. Given the highly endothermic nature of the reforming reactor, heat compensation is achieved by combusting additional methane with air in the reformer furnace. Consequently, according to Feng He (He and Li, 2014), the conventional SMR is estimated to have an overall efficiency of 68.7% (considering LHV). The SMR is crucial to let the SOFC run continuously during the night in case the available green H_2 from the tank is not enough.

2.2.8. *Steam generator*

The Steam Generator (SG) has been modelled as a water tube boiler having an efficiency equal to 90% (Spirax Sarco, 2023). The water tube gas boiler is a heat exchanger designed for the efficient generation of steam. This type of boiler operates on the principle of water circulating through a network of tubes, while hot combustion gases pass over them, transferring heat to the water. The distinctive arrangement of water tubes enhances heat transfer efficiency and allows to produce the saturated steam at a constant pressure of 20 bar requested by the paper mill.

2.2.9. *Gas turbine*

The gas turbine model adopted in this study has been developed and presented in another work by some of the authors. Within that analysis, a traditional GT-powered CHP system is readapted to run with 100% renewable hydrogen, satisfying the energy needs of the same industrial application, for more details the reader is referred to (Mati et al., 2023). An SGT-100 gas turbine manufactured by Siemens (Siemens Energy, 2023) with a nominal electrical power output of 5.4 MW_{el} has been selected as reference case for this study. In order to define the baseline scenario for cogeneration applications, a detailed model of the CHP system has been built using the in-house-developed Energy System Modular Solver (ESMS) modular tool (Carcasci and Facchini, 1996).

A GT component, fuelled with NG, is defined using manufacturer's

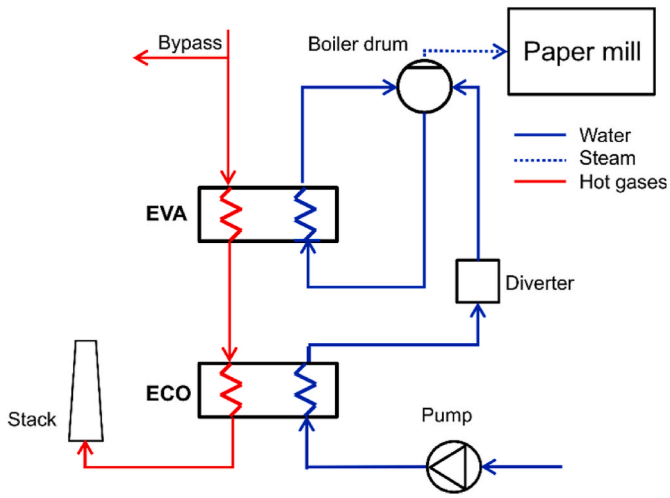

Fig. 4. HRSG schematic diagram.

technical data to match operational design points. The process involves air compression, combustion, and electricity generation during the turbine's expansion phase. Exhaust gases exchange heat with the water-steam circuit in the HRSG section before being released into the atmosphere. The component's geometry and main operational parameters are set based on standard ISO conditions (P_{ISO} = 101325 Pa, T_{ISO} = 15 °C, x_{ISO} = 60%, etc.) allowing to calculate the thermophysical properties of the exhaust gases that are fed as input of the HRSG model design (discussed in the next section). Off-design simulations of the gas turbine are then carried out considering the effects of ambient temperature variations over the year. The main operating parameters are allowed to vary within a predetermined range or constrained by upper as well as lower limits tied to the technological boundaries and environmental regulations. This is the case for the power output, always maintained in a span between 30% and 120% of the rated capacity, while turbine inlet temperature of flue gases is always kept below 1256 °C to comply with the operating limits of materials. The discharge temperature at the stack is also always kept above 105 °C to avoid acid condensation problems related to the sulphur content of the fuel (Zhao et al., 2017).

The resulting operational maps for the cogeneration system, queried at each simulation time step with the facility's thermal load, enable a comprehensive understanding of the turbine's overall performance and accurate assessment of energy load satisfaction and NG consumption.

2.2.10. Heat recovery steam generator

The Heat Recovery Steam Generator (HRSG) has the function of converting the thermal energy of the exhaust gases from either the GT or the SOFC in pressurized saturated steam at a pressure of 20 bar. The configuration considered in this study maintains the same structure for all the investigated cogeneration layouts and it has been modelled as in (Nadir et al., 2016) with two essential components: the economizer and the evaporator. The superheater has not been considered since steam overheating is not necessary for the application considered in the study. In the economizer, the pressurized water at ambient temperature absorbs heat from the hot exhaust gases before entering the evaporator where the phase change occurs through further heat absorption thus leading to the production of saturated steam. As mentioned above, the thermophysical properties of the flue gases constitute the input data set for the HRSG design, together with the steam flow target properties (pressure and vapor fraction). Other crucial parameters are the pinch point temperature difference (ΔT_{pp}), defined as the minimum temperature gap between the hot and cold circuits (maintained at a minimum value of 5 K), and the subcooling temperature difference (ΔT_{sub}) which represents the temperature offset from saturation at evaporator inlet (always $\Delta T_{sub} > 10$ K), in order to avoid boiling phenomena inside the economizer pipes. During system operation, heat demand is always met by using the flue gas diverter at the HRSG inlet when production exceeds demand, or by exploiting the additional steam generator unit in the opposite case.

Fig. 4 represents the HRSG operation. The exhaust gases flow into the evaporator and economizer section to exchange heat with the water-steam circuit, before being released into the atmosphere at the stack. Contemporarily, condensed water returning from the process at ambient conditions is pumped at a pressure of 20 bar. After crossing economizer and diverter sections, water at a temperature of ΔT_{sub} lower than saturation temperature is sent to the boiler drum where steam is generated to satisfy the paper mill thermal demand.

2.3. Economic parameters

In order to evaluate the techno-economic performance of the investigated solutions, two key metrics such as LCOH and NPCs have been considered. These metrics can be used in conjunction to address various aspects of green hydrogen powered energy systems, like it has been done in several studies in the literature (Jang et al., 2022; Marocco et al., 2024; Nicita et al., 2020).

The LCOH metric is extensively adopted in the evaluation of the economic viability of different Power to Hydrogen (PtH) plants by comparing their costs per unit of hydrogen production over the system's lifetime. This indicator represents the point at which the discounted sum of revenues equals the discounted sum of costs, indicating whether the hydrogen market price equals its levelized cost thus allowing to recover the investment within the set period (Fan et al., 2022). All scenarios are assumed to have a timespan (T) of economic operation of 30 years, considering an interest rate (i) of 5 %. The implemented equation is eq. (23):

$$LCOH = \frac{\sum_{y=0}^{T} \frac{(CAPEX_y + OPEX_y)}{(1+i)^y}}{\sum_{y=0}^{T} \frac{H_{2,prod}}{(1+i)^y}} \tag{23}$$

The terms $CAPEX_y$ and $OPEX_y$ in the formula represent namely the annual Capital Expenditures and the annual Operating Expenditures in each year 'y' of the project economic lifetime. These two terms gather the cost expenditures associated with each element constituting the PtH system, namely PV, EL, compressor and H_2 tank. The CAPEX even includes the actualized replacement cost for each technology while the OPEX, since the PtH system runs only on PV production, includes only the Operation and Maintenance (O&M) costs for each technology except for the electrolyzer, which takes into account even the water purchased cost.

It is worth highlighting that the LCOH calculation does not include revenues from the sale of excess PV energy. This exclusion is intended to prevent the PtH system from being oversized for the purpose of selling electricity to the grid (which is not the primary objective of a PtH system). Despite this fact, to have a term of comparison, in results and discussion section even the LCOH with remuneration for the excess PV electricity has been considered.

On the other hand, despite its similarity with the LCOH, the NPC is not related only to the PtH system but rather to all technologies employed in the system over their lifespan, namely PV, EL, compressor, H_2 tank, SOFC, SMR and SG, thus in the NPC formulation the hydrogen production does not appear as represented in eq. (24).

$$NPC = \sum_{y=0}^{T} \frac{(CAPEX_y + OPEX_y)}{(1+i)^y} \tag{24}$$

The NG purchase cost associated with SMR and SG operation is accounted respectively in SMR and SG OPEX. As discussed for the LCOH, the NPC final results do not take into account electricity sold but to have

Table 3
Main economic parameters.

Component	CAPEX	OPEX [€/y]	Lifetime [years]	Reference
PV	690 €/kW	1.29% I_0	25	IRENA (2021)
EL	Cost correlation eq. (26)	Cost correlation eq. (27)	15	(Gorre et al., 2020; Moran et al., 2023)
H_2 Tank (300 bar)	463 €/kg	2% I_0	30	Gallardo et al. (2021)
SOFC	3000 €/kW	2% I_0	15	Cigolotti et al. (2021)
Comp	Cost correlation eq. (25)	2% I_0	20	Mayer et al. (2019)
SG	308 €/kW	1% I_0	30	YongXing Boiler Group (2023)
SMR	280 €/kW	2% I_0	30	(He and Li, 2014; INDEXBOX, 2023; Katebah et al., 2022)

Energy/product stream	Price	Reference
Electricity purchased	200 €/MWh	"Arera: Prezzi e tariffe," (2023)
Electricity sold	65 €/MWh	DOE US (2023)
Water purchased	4 €/Sm3	Marocco et al. (2023)
NG purchased	40.9 €/MWh	"Arera: Dati e statistiche," (2023)

a term of comparison, in results and discussion section even the NPC with remuneration for the excess PV electricity has been considered.

The main economic parameters and assumptions are reported in Table 3:

The PV, SOFC, SG, SMR, H_2 tank and compressor replacement rate is equal to 80 % of the CAPEX, while the EL one is equal to 30 %.

The compressor CAPEX correlation is expressed by eq. (25):

$$CAPEX_{comp} = 0.91 \times 51901 \times \dot{m}_{max,EL}^{0.65} \tag{25}$$

Where $\dot{m}_{\max,EL}$ is the maximum H_2 mass flow rate producible by the electrolyzer.

The electrolyzer CAPEX correlation is expressed by eq. (26):

$$CAPEX_{EL} = 1185 \times P_{EL}^{0.925} \tag{26}$$

While the electrolyzer O&M correlation is given by eq. (27):

$$O\&M_{EL} = \left(349.8 \times P_{EL}^{-0.305}\right) \times P_{EL} \tag{27}$$

The baseline scenario for NG purchase price in the market, useful to calculate the NPC associated with SG and SMR technologies, was established at 40.9 €/MWh, as determined by the Italian Energy Networks and Environment Regulatory Authority (ARERA), specifically outlined in the Natural Gas End Prices for Industrial Consumers ("Arera: Dati e statistiche," 2023). The baseline scenario for electricity sale price in the market was established at 65 €/MWh as assessed by the most recent wholesale energy prices under the Power Purchase Agreement (PPA) schemes adopted in (DOE US, 2023).

2.4. Study case

Comparative analysis focuses on three cogeneration alternatives: a conventional natural gas-powered GT (named GT configuration from now on) schematized in Fig. 5, a SOFC using grey hydrogen from a SMR (named S1 configuration from now on) schematized in Fig. 6, and an advanced SOFC operating on on-site produced green hydrogen (named S2 configuration from now on). The latter involves an integrated multi-energy system with PV panels, electrolyzers, compressors, and storage tanks schematized in Fig. 7.

The conventional GT cogeneration system, currently employed in the paper and mill industry, adequately addresses both electric and gas loads using the thermal follow logic. Any shortfalls in electric load coverage are supplemented by the electricity grid, while deficiencies in meeting the thermal load are compensated for by a SG.

The SOFC operating with hydrogen, emerges as a viable alternative to the GT cogeneration system. This is attributed to its capability to operate at high temperatures, delivering high electric efficiency in both nominal and off-design conditions. In S1 configuration, the study aims to assess the economic and environmental implications (specifically, CO_2 emissions) of a SOFC cogeneration system relying solely on grey hydrogen, produced through a SMR. Since the SOFC has a higher electric efficiency than the GT, instead of using the thermal follow logic, the electric follow logic is implemented. To maintain parity with the existing GT system, the SOFC's size remains the same, and any gaps in electric load coverage are bridged by the electricity grid. Notably, due to the lower thermal efficiency of the SOFC compared to the GT, a larger SG is required to meet the remaining thermal load.

S2 configuration, the focal point of detailed analysis in this paper, offers a pathway for partial decarbonization of energy-intensive industries. In this setup, the SOFC operates with a combination of grey hydrogen (produced by the same SMR) and green hydrogen (produced by an on-site H_2 production plant relying only on a PV field). Differently from the previous configuration, the SOFC does not run continuously; instead, during sunny hours, the electric load is primarily met by the PV system, with surplus energy used to produce hydrogen via a PEM electrolyzer. The produced hydrogen is then compressed and stored in an H_2 tank. Consequently, the SOFC is activated only when solar energy is

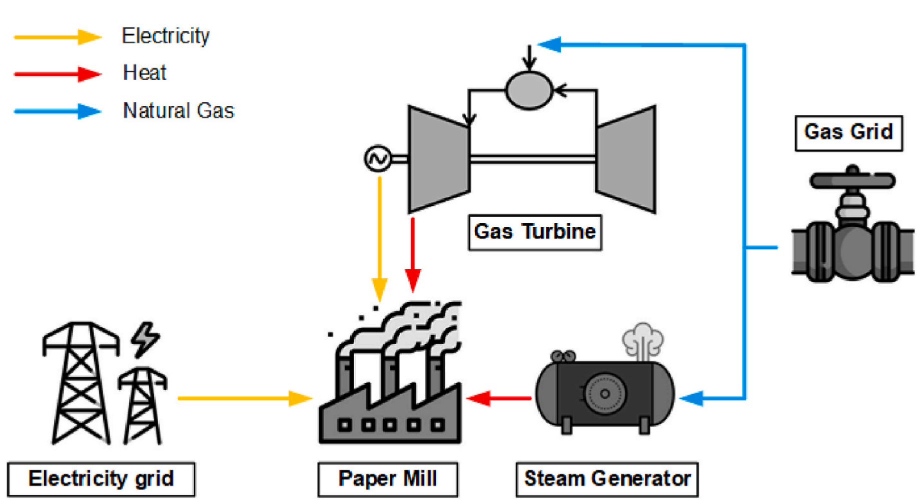

Fig. 5. Schematic diagram of GT configuration.

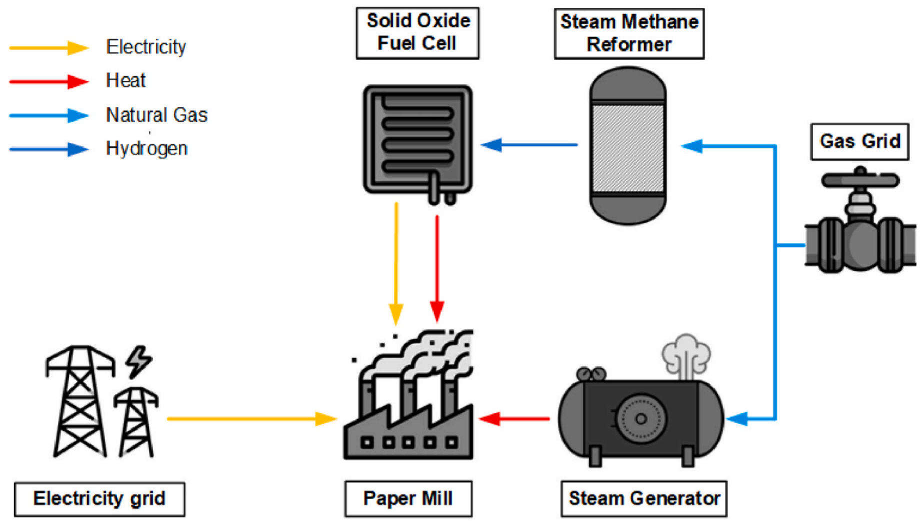

Fig. 6. Schematic diagram of S1 configuration.

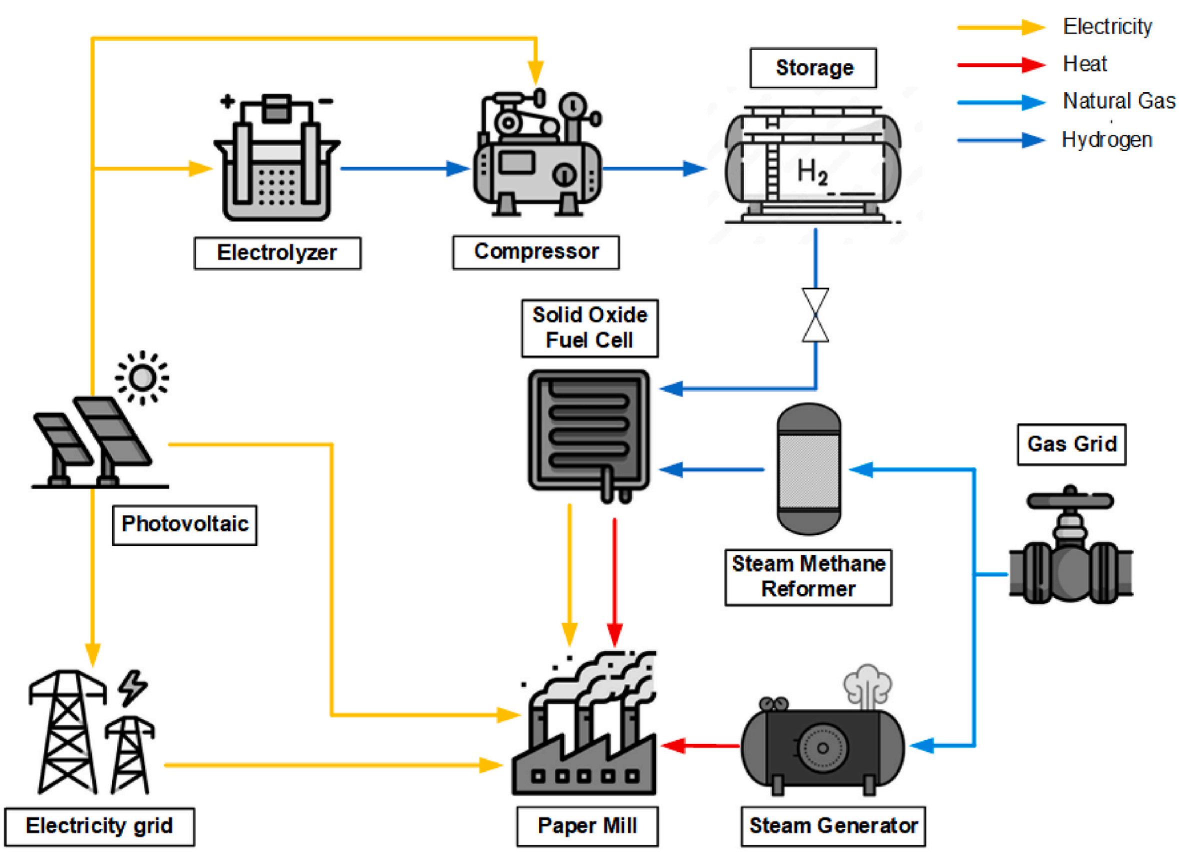

Fig. 7. Schematic diagram of S2 configuration.

insufficient, prioritizing the use of stored green hydrogen and resorting to grey hydrogen from the SMR as a secondary option.

The SOFC has a prolonged start-up time, but as outlined in the Materials and Methods section, new solutions are continuously developed, and the start-up phase can be notably reduced. This enables the SOFC to be shut down and restarted on a daily basis, even though this may lead to a shorter lifespan due to accelerated aging. The reliance on PV during the day means that the thermal load to be addressed during sunny hours is significantly higher. Consequently, a larger SG size is necessary to compensate for SOFC's limitations in covering the thermal load, especially when the SOFC is not operational.

2.4.1. Simulation assumptions and constraints

As explained in the previous section, the required size for the SG in the GT configuration is less than that in configurations incorporating the SOFC. In the GT setup, the SG, complementing the GT itself, is sized at 3.5 MW_{th}, whereas in the S1 configuration, it necessitates a size of 12.7 MW_{th}. The sizing of the SMR, following common practice in scientific literature (He and Li, 2014), is defined based on output power, coinciding with the input power of the SOFC, and consequently set at 10.8 MW_{th}.

In S2 configuration, both the SOFC and SMR sizes remain consistent with the previous configuration. However, the SG size is increased from

Table 4
Auxiliary components of the main cogeneration technologies for the different configurations.

Configuration	Component	Parameter	Units	Value
GT GT connected to a HRSG and an auxiliary SG.	SG	Input Power	[MW_{th}]	3.5
GT powered with NG		Efficiency	[%]	90
S1 SOFC connected to a HRSG and an auxiliary SG.	SG	Input Power	[MW_{th}]	12.7
		Efficiency	[%]	90
SOFC powered with grey H_2	SMR	Output Power	[MW_{th}]	10.8
		Efficiency	[%]	68.7
S2 SOFC connected to a HRSG and an auxiliary SG.	SG	Input Power	[MW_{th}]	15.2
		Efficiency	[%]	90
SOFC powered with both grey and green H_2	SMR	Output Power	[MW_{th}]	10.8
		Efficiency	[%]	68.7
	PV	Input Power	[MW_{el}]	Optimized
		Tilt	°	30
		Azimuth	°	0
		Losses	%	14
		Ref. year	–	2015
	EL	Input Power	[MW_{el}]	Optimized
		Single module power	[MW_{el}]	0.2
		Operating pressure	bar	30
		Efficiency	kWh/Nm^3	4.55
	Comp	Input Power		Optimized
		Pressure inlet	bar	30
		Pressure outlet	bar	300
		Efficiency	kWh/kg_{H2}	2.02
	H_2 Tank	Size	tons	Optimized
		Operating pressure	bar	300

12.7 to 15.5 MW_{th} to adequately meet the highest hourly thermal demand. The on-site hydrogen production and storage plant is optimized to achieve the minimum LCOH. Specifically, various combinations of PV and EL sizes are systematically investigated in this study. The EL is composed of a stack comprising 200 kW modules, with scalability achieved by increasing the number of these modules. The compressor is sized to accommodate the maximum hourly hydrogen flow producible by the electrolyzer, and the tank is designed to store hydrogen production equivalent to 8 h of uninterrupted operation, enabling daily storage. This setup fills the tank during daylight hours and depletes it overnight, maximizing the utilization of power supplied to the EL from the PV field. While an alternative approach to compensate for the annual variation in PV production would involve using a larger tank, allowing the system to fill the tank during the summer and empty it during the winter, the authors intentionally chose to size the tank for daily storage, a decision primarily influenced by economic factors as substantiated by existing scientific research (Marocco et al., 2024; Mati et al., 2023; Moran et al., 2023).

The parameters describing the auxiliary components of the main cogeneration technologies for the different configurations are highlighted in Table 4.

2.4.2. *Workflow*

The workflow of the proposed plant is a rule-based algorithm designed to efficiently meet both the electrical and thermal demands of the paper mill industry, taking into account varying PV sizes, electrolyzer scales, and storage capacities. The primary objective is to satisfy a medium electric load of 5 MW_{el}, requiring the SOFC to be supplied with 292 kg/h of hydrogen under nominal conditions.

To achieve this, a continuous input of 15 MW_{el} electrical power to the electrolyzers is necessary if relying solely on green hydrogen production. However, due to the inherent intermittency of PV field production, electrolyzers with higher nominal power are installed to generate a hydrogen surplus during electricity production peaks. This surplus is stored for later use. The SOC of the storage tank is updated at every simulation timestep.

Prioritizing the direct use of PV-generated electricity to meet the electrical load is crucial before contemplating hydrogen production. This is because employing PV-generated electricity for hydrogen production, which is then used in a SOFC for reconversion into electricity, results in avoidable energy losses. Therefore, a parametric control strategy is applied to simulate system behavior when integrating all components.

The flow chart in Fig. 8 illustrates the control strategy managing power and hydrogen fluxes at each timestep (i). The key inputs are the current PV field production (P_{PV}) and the electric and thermal load requests from the paper mill (P_{el_load}, P_{th_load}).

At each hour, PV is activated. If the PV power exceeds the electric load, the SOFC remains inactive. The surplus PV power (P_{sur}) is directed to the electrolyzer to produce green H_2, which is then compressed using the remaining PV surplus. An iterative process ensures both the electrolyzer and compressor operate solely on PV surplus power. Neither the electrolyzer nor the compressor uses electricity from the grid. The compressed H_2 is stored in the tank, and the thermal load is covered by a SG. Any remaining surplus is injected into the electricity grid.

If the PV power is insufficient or zero, the SOFC is activated using the green H_2 stored in the tank. If H_2 in the tank is not enough, a SMR is employed to produce grey H_2, enabling the SOFC to meet the entire electric load. If the electric load persists, it is supplemented by electricity from the grid. As a cogeneration system, the SOFC generates thermal power, covering the required thermal load. If there is excess thermal power, the process concludes; otherwise, a SG compensates for any deficiencies in thermal load coverage by the SOFC.

2.4.3. *Hourly balances*

The hourly energy balances of the system under investigation are modelled utilizing the Multi-Energy System Simulator (MESS), an open-source computational modelling tool developed by the authors' research group designed for analytical purposes as described in (Lund et al., 2021). For more information on the structure and simulation logic of MESS, the reader is referred to refs. (Bottecchia et al., 2021; Lubello et al., 2022). SOFC technology model described in the modelling section has been therefore implemented and added as new feature into this tool to run hourly simulations following the logic described above.

Fig. 9 illustrates the temporal evolution of key parameters in a configuration involving 20 MW_{el} of electrolyzers, a H_2 tank with a capacity of 3.2 tons designed to accommodate 8 h of continuous H_2 production, a 40 MW_{el} PV system, a 5.4 MW_{el} SOFC, a 1.1 MW_{el} compressor, a 10.8 MW_{th} SMR, and a 15.5 MW_{th} SG. The plot covers the initial two weeks of three different months on an hourly basis.

The variation trends are depicted by specific lines and bars representing SOC of the H_2 tank (blue line), grey H_2 production by the SMR utilized by the SOFC to meet electric demand (dashed grey line), and power variations for the various technologies considered (represented by multiple bars in the plot). It is noteworthy that grid support is seldom required, as the electric load rarely exceeds 5.4 MW_{el}.

The black line in the plot represents the total electric load, comprising electric, electrolyzer and compressor demand. This load is met by the PV system and SOFC. Any surplus power generated by the PV system is injected into the grid.

The SOC of the H_2 tank fluctuates between the minimum and maximum values due to its designed daily storage function. The grey dashed line represents the periods when the tank is empty, prompting the SMR to produce grey H_2 to sustain continuous operation of the SOFC.

The analysis considers three distinct scenarios over a period of three

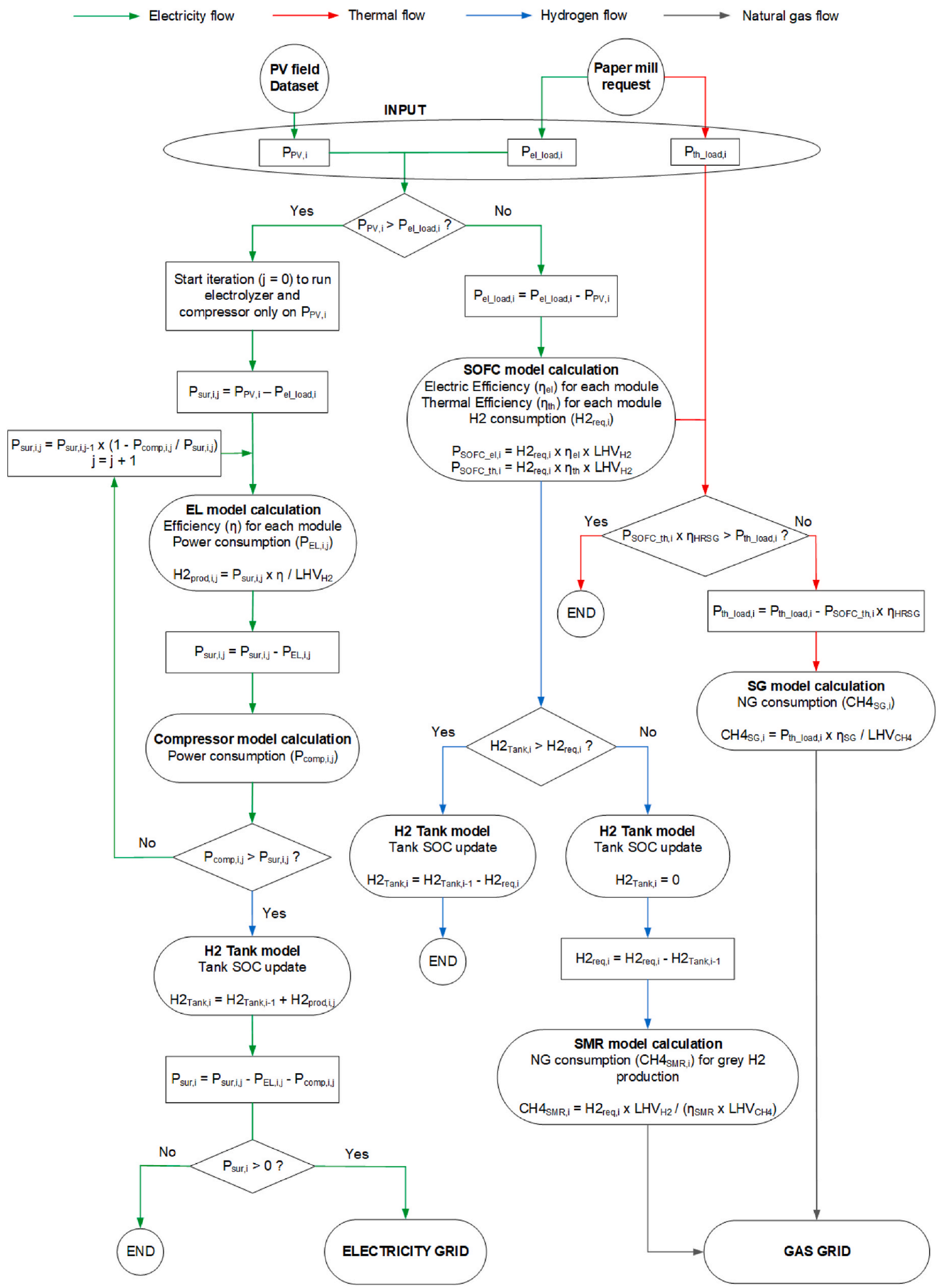

Fig. 8. Workflow: S2 configuration operating logic.

months.

a) February: This period reflects a medium-high SMR-dependent operation. Low PV production at the beginning and end of the two weeks results in an almost empty tank. Subsequently, as high PV production occurs from the 7th to the 13th day, the system operates more autonomously, increasing the daily production of green H_2 by electrolyzers and reducing reliance on grey H_2 from the SMR during the night.

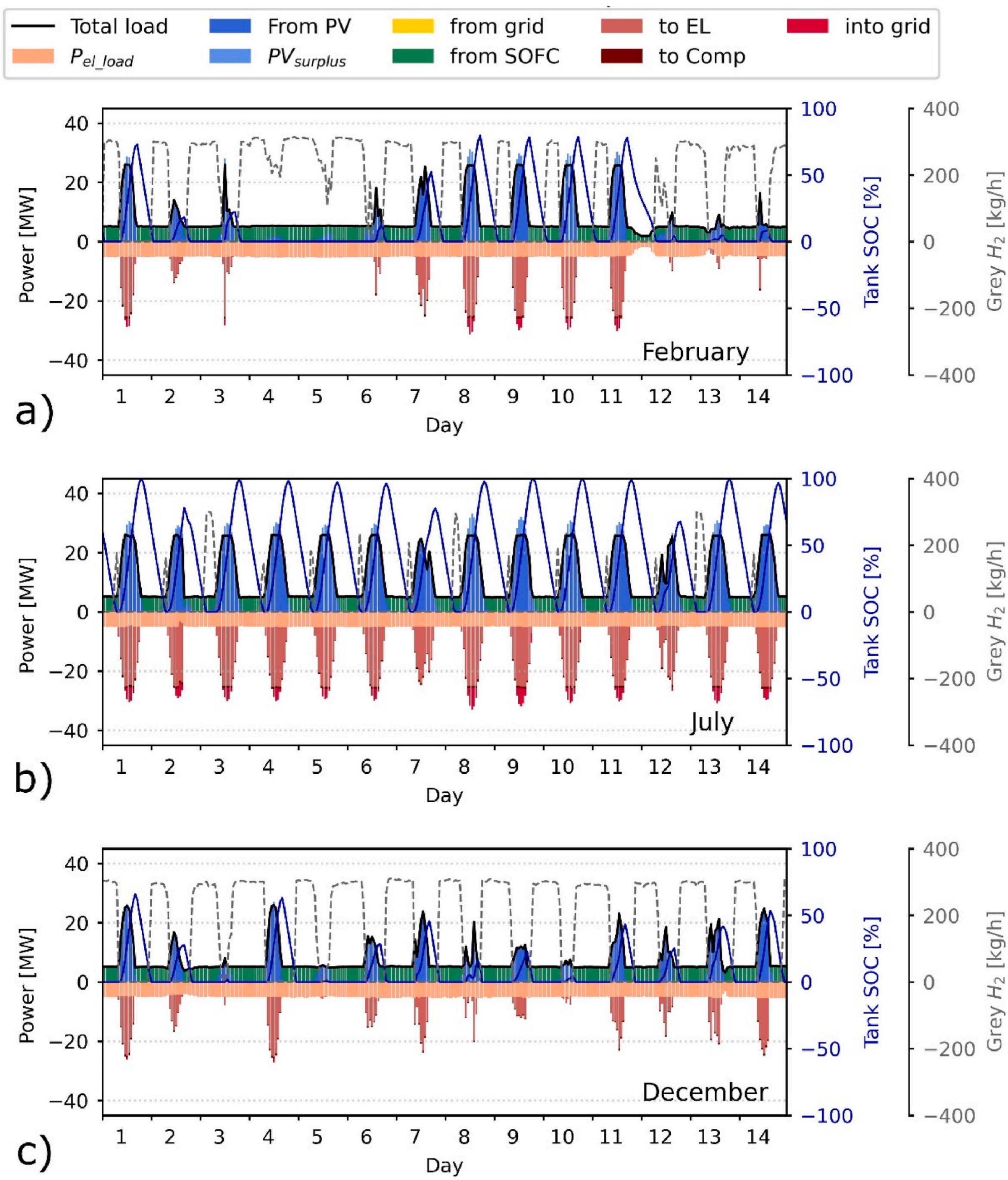

Fig. 9. Power balances, Tank SOC and grey H_2 production trend during two weeks of operation. February (a), July (b), December (c).

b) July: This represents an example of high self-sufficiency. Throughout the two weeks, the electrolyzers operate at nominal power for nearly 8 h every day, allowing the tank to be filled by the end of daytime. Consequently, the system is largely independent of the SMR during the night. Additionally, the PV system covers the electric load during the day, thus reducing SOFC operating hours.
c) December: This scenario exemplifies high SMR-dependent operation. The low PV power production during the day in the first two weeks of December consistently activates the SMR for more than 12 h per day, emphasizing the system's reliance on grey H_2 production during this period.

3. Results and discussion

In this section, the performance comparison between SOFC and GT is initially conducted, detailing the physical interactions between their output mass flow rates and the HRSG in producing high-temperature pressurized steam. Following this, the outcomes of the comparative analysis among the three distinct configurations outlined in section 2.4 are presented in terms of key economic and environmental parameters. Finally, a sensitivity analysis on the electricity sale price and NG purchase price is performed.

Table 5
Main parameters of the investigated cogeneration technologies: GT and SOFC.

Parameter	Units	CHP	
		GT	SOFC
Output electric power	[MW_{el}]	5.4	5.4
Electric efficiency	[%]	30.2	50.5
Input thermal power	[MW_{th}]	17.8	10.8
Exhaust temperature	[°C]	549	800
Exhaust mass flow	[kg/s]	21	2.6
		HRSG	**HRSG**
HRSG efficiency	[%]	99%	99%
Subcooling	[°C]	10	75
Pinch Point	[°C]	5	10
Stack temperature	[°C]	105	105
		GT + HRSG	**SOFC + HRSG**
Steam generated	[kg/s]	3.97	0.98

3.1. GT and SOFC coupling with HRSG

In the GT configuration, the GT is sized at 5.4 MW_{el} as it has been done in a previous study by the authors (Mati et al., 2023). To maintain alignment with the existing GT system, the SOFC is also sized at 5.4 MW_{el} (a stack composed by 54 modules of 100 kW). However, there are important differences between their performances, as well as their coupling with the HRSG to produce saturated steam at a constant pressure of 20 bar (212 °C).

The performance comparison between GT and SOFC is represented in Table 5. Based on the technology modeling presented in the methodology section, for an equal power output of 5.4 MW_{el}, the GT demonstrates an electric efficiency of 30.2%, while the SOFC achieves 50.5%. Consequently, considering fuels lower heating value, the input thermal power is respectively 17.8 MW_{th} and 10.8 MW_{th}.

To assess the thermal output power convertible in pressurized steam some considerations must be done. Under nominal conditions, the composition and characteristics of the exhaust flows destined for the HRSG differ significantly between the GT and SOFC. The GT exhaust flow comprises 20.9 kg/s of flue gases with a mass fraction of 75% nitrogen, 23% oxygen, and negligible amounts of water vapor and CO_2. This mixture is at a temperature of 549 °C and atmospheric pressure. In contrast, although the SOFC produces a significant amount of internal heat, a substantial portion is utilized to heat the inlet air and H_2, allowing the SOFC to maintain a temperature of 800 °C. As a result, the total mass flow rate of the SOFC exhaust is 2.6 kg/s, which is lower than that of the GT. This exhaust consists of air exiting from the cathode, predominantly nitrogen without oxygen, and water vapor exiting from the anode, with mass fractions of 65% and 35%, respectively. The exhaust occurs at a temperature of 800 °C and atmospheric pressure. Unlike the GT, where there is a single gas stream, in the SOFC, air and water vapor are mixed before entering the HRSG.

Fig. 10 illustrates the T-Q diagram depicting the heat exchange between the hot exhaust flows and the water steam circuit within the HRSG for both configurations. Assuming a consistent HRSG efficiency of 99% in terms of heat exchanged between exhaust flow and water, key HRSG operating parameters are presented in Table 5.

The main distinction lies in the fact that the SOFC exhaust gases at near-atmospheric pressure contain a higher amount of vapor, whose latent heat cannot be converted into saturated steam at 20 bar because the stack temperature must exceed 100 °C to avoid corrosion problems that can be generated by water vapor condensation. This factor, coupled with a lower SOFC output mass flow rate than GT (slightly mitigated by the higher output temperature) implies that the generated pressurized steam is only 24.6% compared to the GT case.

Consequently, the thermal efficiency of the system is 25%, leading to a total system efficiency of 75.5%. These results align with existing scientific literature. For example, Pirkandi et al. found an overall SOFC–CHP system efficiency of about 73% (Pirkandi et al., 2012). Cinti et al. investigated the performance of SOFC–CHP systems with fuels ranging from pure hydrogen to pure methane, finding that while natural gas-based systems exhibit higher electrical efficiency, the introduction of hydrogen increases the total efficiency to values as high as 80% (Cinti et al., 2019).

This underscores a crucial point for the envisaged scenarios, necessitating substantial compensation by the SG when the CHP system employs the SOFC.

3.2. GT, S1 and S2 configuration comparison

This section presents the outcomes of the comparative analysis among the three distinct configurations outlined earlier. GT and S1 configurations have fixed component sizes, while S2 underwent an in-depth parametric analysis to determine the optimal techno-economic-environmental configuration. This involved assessing the variations in three key parameters: one environmental (NG consumption in relation to the existing GT configuration) and two economic. The economic parameters include NPCs and the LCOH for both green (produced from the EL) and grey (produced from the SMR) hydrogen.

Fig. 11 displays the hourly thermal and electric load profiles for the second week of May across three discussed configurations. Additionally, it provides corresponding technology profiles associated with each configuration. In the GT one, the paper mill is powered by a 5.4 MW_{el} GT (operated in thermal-follow mode) and a 3.5 MW_{th} SG. S1 configuration involves a 5.4 MW_{el} SOFC (operated in electric-follow mode) and a 12.7 MW_{th} SG while in S2 configuration a PtH plant is introduced, with the paper mill being powered by a 5.4 MW_{el} SOFC fuelled by both green and grey hydrogen, a 40 MW_{el} PV system, and a 15.2 MW_{th} SG. The third configuration also includes a green hydrogen production and storage plant, comprising a 20 MW_{el} EL, a 1.1 MW_{el} compressor, and a 3.2 tons

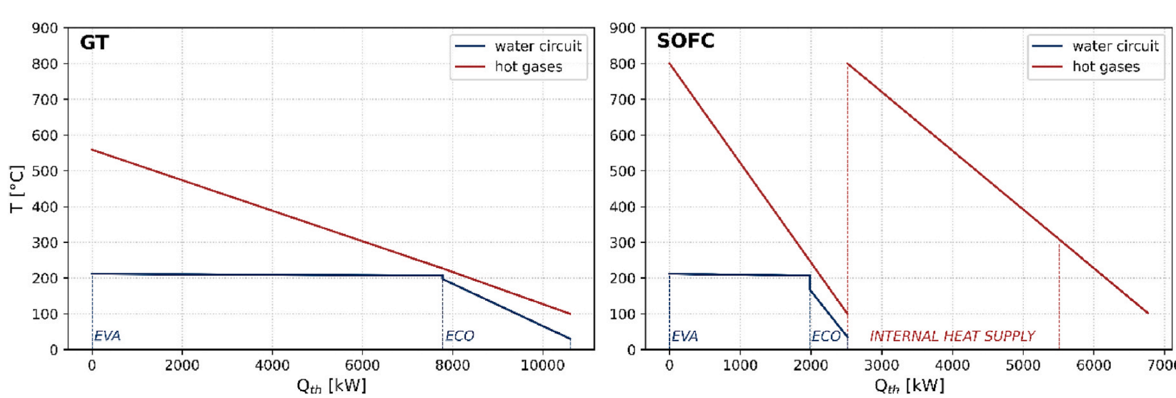

Fig. 10. HRSG temperature-heat diagram.

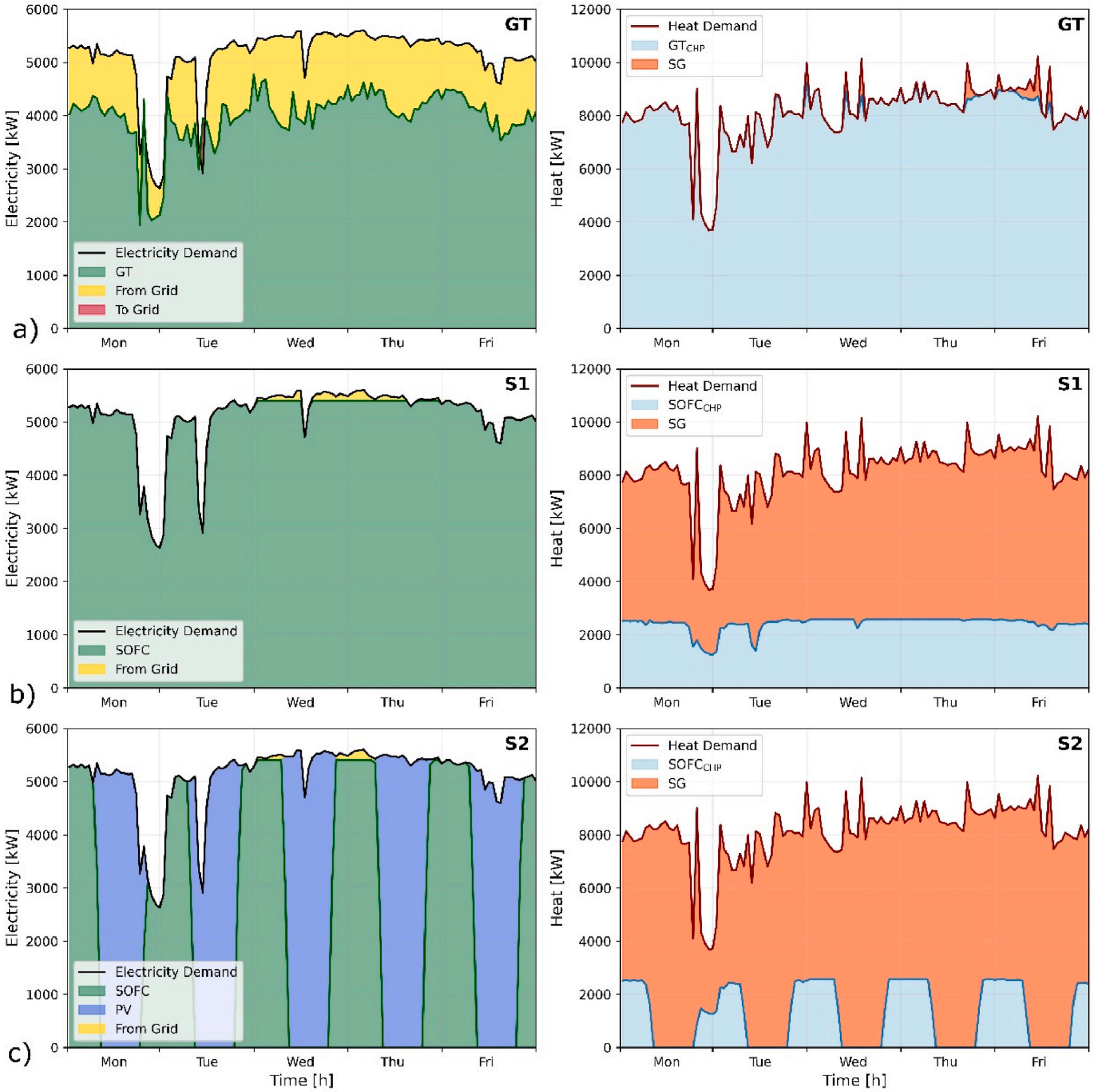

Fig. 11. Hourly thermal and electric load profiles for the second week of May across three discussed configurations: a) GT configuration, b) S1 configuration, c) S2 configuration.

tank capacity. In all three configurations, any deficits in meeting the electric load are compensated by the electricity grid.

Main annual energy outcomes are summarized in Table 6. GT configuration results are based on a previous study by the authors (Mati et al., 2023).

Table 6 and Fig. 11 shed light on the prevailing use of GTs in the paper mill industry today. This sector, being energy-intensive, has a thermal load that is approximately twice its electrical counterpart. This characteristic makes the GT an optimal choice due to its high thermal efficiency, which satisfies 93% of the paper mill steam demand and 85% of the electric load, consuming 10915 tons of NG annually. On the contrary, the SOFC, despite its equivalent size to the GT, exhibits elevated electric efficiency paired with diminished thermal efficiency, resulting, as expressed in section 3.1, in a substantially reduced pressurized steam output from the HRSG. Therefore, the SG becomes imperative to address the thermal deficiencies of the SOFC. In fact, in the S1 configuration, where the SOFC operates continuously working with the electric follow logic, it successfully covers 99.9% of the electric load but only 26% of the thermal one. This is achieved using 2561 tons of grey H_2 by SMR which uses 9424 tons of NG. Simultaneously, the SG necessitates an additional 4992 tons of NG to compensate for the thermal deficiencies of the SOFC. As a result, total NG consumption is 32% higher than that of the GT configuration.

So, even when exclusively utilizing 100% green H_2 in the SOFC (thus mitigating the consumption of 9424 tons of NG), achieving complete decarbonization in this industry remains unfeasible due to the indispensable requirement for the SG to cover the residual thermal load. The residual thermal load could be decarbonized by operating the SG on green H_2 instead of NG. However, this would necessitate additional hydrogen production, leading to an increase in overall system size while a more practical solution might be to replace the SG with a heat pump, which could offer greater efficiency.

In S2 configuration, PV covers 38% of the electric load, generating an electricity surplus enabling the production of 701 tons of green H_2. To meet the remaining electric load, the SOFC relies on SMR to produce an additional 853 tons of grey H_2, predominantly during periods of decreased PV production in the winter, as comprehensible by Figs. 9 and 11. The SG experiences increased operation in comparison to S1 configuration, as during sunny hours when PV production fulfills the electric load, the SOFC remains inactive, necessitating the SG to entirely

Table 6
Main annual energetic outcomes.

	Electric load fulfillment [%]	Thermal load fulfillment [%]	NG used [t]	Grey H_2 [t]	Green H_2 [t]
GT					
GT	85.35	93.11	10452	–	–
Electricity grid	14.65	–	–	–	–
SG	–	6.89	463	–	–
S1					
SOFC	99.96	26	9424	2561	0
Electricity grid	0.04	–	–	–	–
SG	–	74	4992	–	–
S2					
SOFC	61.14	16	3137	853	710
PV	38.84	–	–	–	–
Electricity grid	0.02	–	–	–	–
SG	–	84	5675	–	–

cover the thermal load. Consequently, 8812 tons of NG are used, reducing total NG consumption by 20% compared to the GT configuration.

The subsequent section offers an in-depth exploration of the techno-economic-environmental outcomes associated with S1 and S2 configurations.

3.2.1. S2 configuration optimization

This section presents a comprehensive analysis of the multi-energy system under investigation. Employing a simulation-based optimization strategy, the study wants to identify the optimal techno-economic-environmental configuration by examining variations in three key parameters: NG consumption, LCOH, and NPCs.

Specifically, the optimization process focuses on sizing the PV system, EL, compressor, and H_2 tank to achieve the minimum LCOH. Notably, the sizes of the compressor and tank are intricately linked to the electrolyzer's size. As outlined in Section 2.4.1. , the compressor is dimensioned to manage the maximum hydrogen flow rate producible by the electrolyzer while the H_2 tank is sized to accommodate 8 h' worth of uninterrupted hydrogen production allowing for daily storage.

Fig. 12 highlights main energetic and economic results varying PV and EL capacity. The values obtained for PV size equal to zero corresponds to S1 configuration results because it means that no PtH plant is employed.

In Fig. 12a, it is observed that an increase in the PV field size leads to a decrease in the SOFC Capacity Factor (CF), regardless of EL size. The SOFC CF drops from 92% (correspondent to S1 configuration value) to a value of 50%. This is attributed to the larger electric load covered by a higher PV size. Consequently, as the SOFC operates in electric-follow mode, its covered electric load decreases from 99% to 55%, while the covered thermal load decreases from 26% to 14%. The electrolyzer CF also varies, but just up to a maximum of 30%. This is because the EL is activated only when a surplus is available from PV, resulting in the EL being turned off even during hours of low production.

In Fig. 12b, it is noted that the trend in grey hydrogen consumption is the mirror image of green hydrogen consumption. Green hydrogen consumption for SOFC feedstock ranges from zero (S1 configuration value) to 1400 tons, while grey hydrogen consumption ranges from 2561 (S1 configuration value) to 5 tons. This is due to the increase in green hydrogen production with larger PV and EL sizes, reducing the need for grey hydrogen produced by SMR and contributing to industrial decarbonization. The decision to size the storage tank for daily storage makes it impossible to reach zero tons of grey hydrogen production, as seasonal storage would incur significantly higher costs.

Fig. 12c depicts the behavior of green and grey LCOH. The latter increases with PV and EL size because the reduced production of grey hydrogen leads to a lower amortization of SMR costs. Conversely, green LCOH exhibits a minimum within a specific range of PV (38–60 MW_{el}) and EL (18–30 MW_{el}) sizes. This suggests that as the availability of renewable resources increases, there is enhanced exploitation of the installed electrolytic potential, improving its CF. However, beyond a certain point, the higher green hydrogen production obtained with larger PV and electrolytic sizes may not justify the increased investment costs associated with these technologies, identifying a minimum value for green LCOH.

Fig. 13 provides insights into the variations in NPCs, LCOH, and NG consumption in relation to the GT configuration. These variations are observed by varying the percentage of grey hydrogen used to operate the SOFC. Each bar in the figure represents the plant configuration associated with the minimum LCOH for the specified percentage of grey H_2 utilization.

As detailed in section 2.3, the NPCs of the technologies encompass both capital costs and actualized O&M costs. For the SMR and the SG, the NPC is augmented by the NG cost required to operate them. This is because the purchase cost of NG is treated as an operational cost associated with these technologies. Consequently, in the electrolyzer NPC is included even the cost of purchased water used in the process.

Fig. 13a shows the breakdown (in opposite directions) of the NPC and NG utilization for different values of grey hydrogen share. 100% grey H_2 share corresponds to S1 configuration where no PtH system is involved, thus if the NPCs are the lowest and associated mainly with the SMR, NG consumption (14416 tons) is 32% higher than the current GT scenario, while 0% grey hydrogen share means that no SMR is necessary. For values above 60% of grey hydrogen share, the NPCs associated with SG and SMR represent the largest cost contribution while for the other scenarios the PtH components (mainly PV and EL) have the largest impact. Moreover, it is evident that with the transition to lower values of grey hydrogen share, the revenues associated with the surplus electricity exported to the grid increase significantly ("Grid export" area) because of the sharp increase in the PV size. Finally, it is noteworthy that the storage system is an important cost contribution (7%) in the fully decarbonized scenario (almost 0% grey hydrogen share), in which a large tank (28 tons) is required to ensure a reliable supply of green hydrogen throughout the year. These findings are consistent with those reported in (Trapani et al., 2023), where a fixed price for grey hydrogen is utilized instead of producing it internally via a SMR. It is important to highlight that complete decarbonization of the paper mill is not achievable, specifically, the consumption of NG can only be reduced by up to 50% compared to the current GT configuration. The remaining 50% of NG consumption is essential for the SG, which serves the crucial role of compensating for SOFC limitations in meeting the thermal load requirements.

Fig. 13b shows the grey LCOH and the green LCOH – and how it is distributed among the PtH components – for different values of grey hydrogen share. Two different scenarios were considered:

Scenario 1 (black-edge squares): There are no revenues for the excess renewable energy.

Scenario 2 (blue-edge triangles): The excess renewable energy is remunerated, and the electricity sale price is set equal to 65 €/MWh as assessed by the most recent wholesale energy prices under the PPA schemes adopted in Italy (DOE US, 2023).

For 0% grey H_2 share the green LCOH of Scenario 1 amounts to 14.2 €/kg (black-edge square), which is the highest LCOH value among all the configurations analyzed. This high cost is due to a considerable oversizing of the PV plant (light green area), the EL (light blue area) and the H_2 tank (blue area). Regarding Scenario 2, a remuneration for the excess PV energy results in a reduction of the green LCOH to 8.5 €/kg (blue-edge triangle). Then the green LCOH progressively decreases as both PV and EL size decrease. The minimum LCOH is achieved when there is an

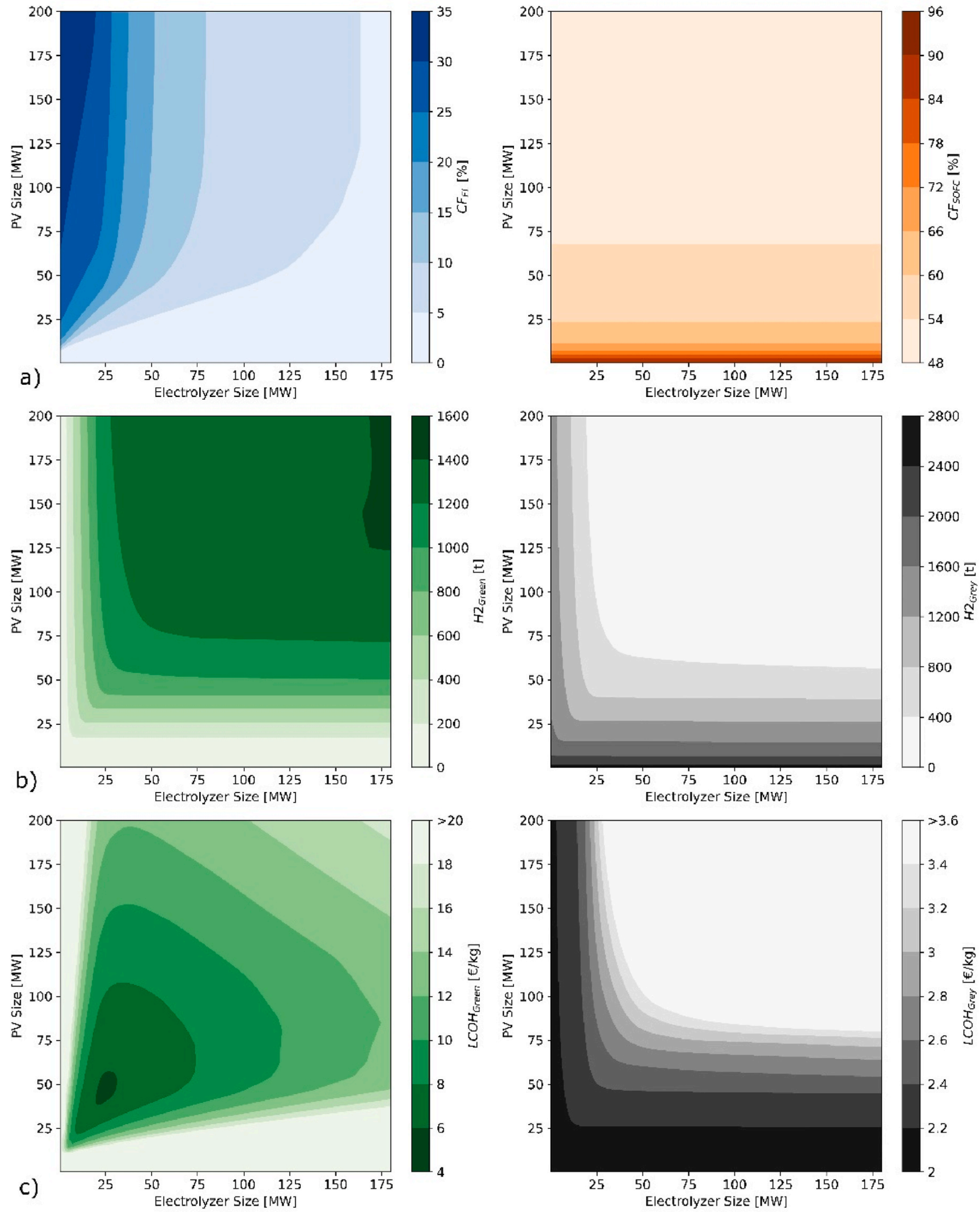

Fig. 12. S2 configuration. a) EL and SOFC capacity factor, b) total green and grey H_2 produced, c) green and grey LCOH varying PV and EL capacity.

optimal balance among the costs of PV and EL technologies, the capacity factor of the electrolyzer, and the quantity of green hydrogen produced, and this happens for 40% grey H_2 share and corresponds to 5.81 €/kg (down to 5.26 €/kg when considering electricity sold revenues). Then the green LCOH progressively increases because the reduced size of PV and EL is not justified by the lower amount of green hydrogen produced. Instead, the grey LCOH always decreases, because the less grey hydrogen is produced the less the cost of the SMR is amortized.

The range of green hydrogen production costs determined in this study (from 5.2 to 10 €/kg) is slightly higher than the broad spectrum of production costs for PV-based PtH systems found in the literature because PV first task is to cover the electric load rather than feeding the electrolyzer. Hofrichter et al. (2023) evaluated the LCOH of PV-based hydrogen production systems at different geographical locations (with different solar potentials and PV capacity factors). They computed values in the range 3.1 ÷ 5.9 €/kg for countries with high solar potential and 4.1 ÷ 9.6 €/kg for those with low solar potential. Similar hydrogen production costs were also reported by Bhandari and Shah (2021), who collected several case studies from the literature about PEM electrolyzer-based PtH systems and found a median LCOH value of 5.1

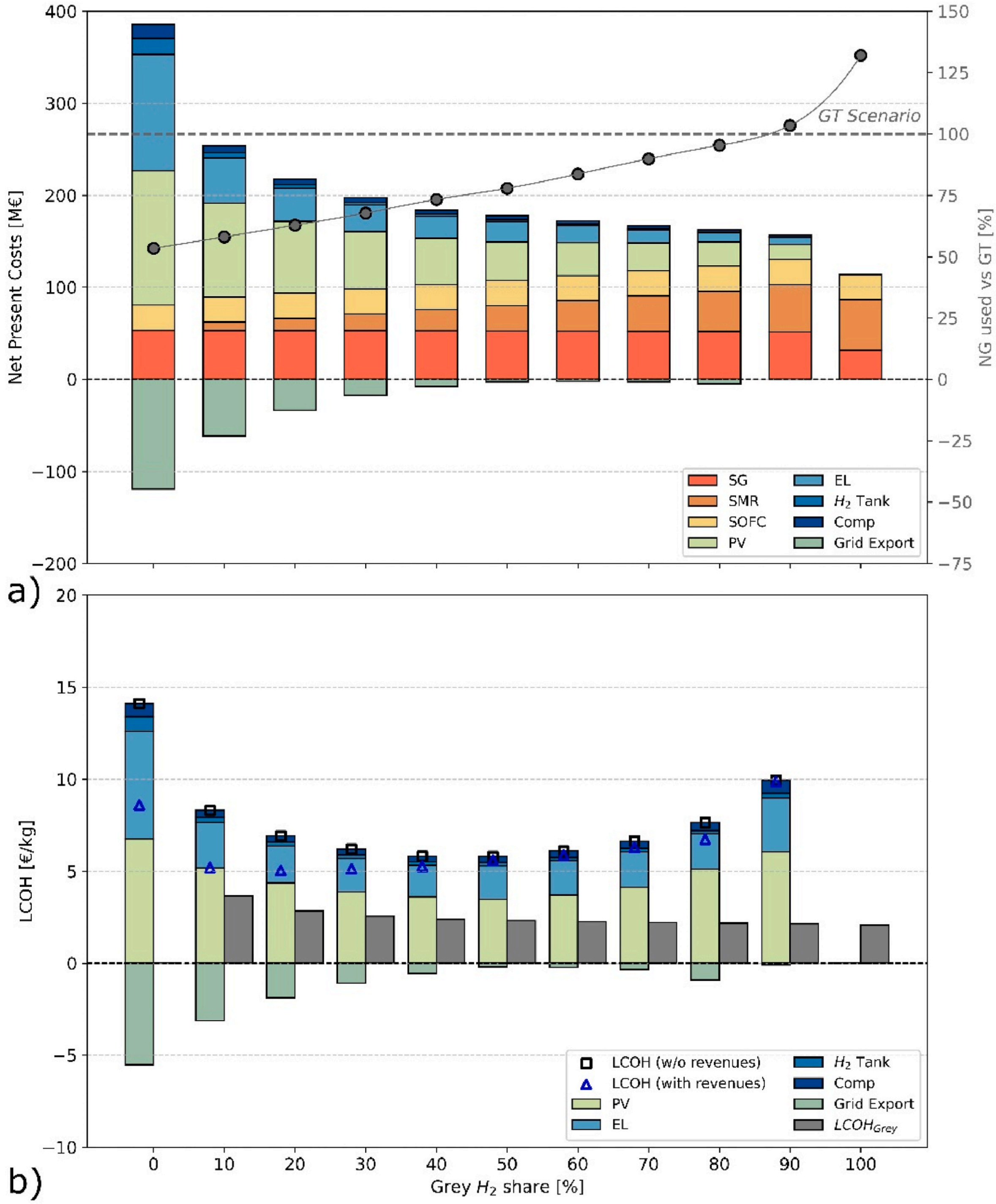

Fig. 13. a) NPC and NG consumption breakdown, and b) grey LCOH and the green LCOH trend for different values of grey hydrogen share. Two main scenarios are analyzed: 1) no remuneration for the excess PV electricity (black-edge squares), and 2) the electricity sale price is set equal to 65€/MWh (blue-edge triangles).

€/kg.

Thus, the optimal techno-economic-environmental configuration, namely the one having the minimum LCOH equal to 5.81 €/kg, is reached for a 38% grey H_2 share and a 50.6 MW_{el} PV, a 25.2 MW_{el} EL, a 1.4 MW_{el} compressor, and a 3.9 tons H_2 tank leading to the abatement of 25% of current NG consumption in the GT scenario.

The optimal PV-to-electrolyzer ratio (PV/EL ratio), defined as the ratio of PV system size to electrolyzer capacity, is found to be 2. This result is consistent with existing scientific literature on PV-based PtH systems. For instance, Abdin et al. reported optimal PV/EL ratios ranging from 1.8 in Los Angeles, USA (a region with high solar potential), to 3.1 in Adelaide, Australia (a region with lower solar potential) (Abdin and Mérida, 2019). Similarly, Yates et al. conducted an uncertainty analysis on hydrogen electrolysis from off-grid standalone PV systems in Townville (Australia), identifying an optimal PV oversize ratio of 1.5 (Yates et al., 2020).

As a result, this type of configuration may be ideally suited for energy-intensive industries with a higher electric than thermal load. In such industries, the SOFC could represent a solution to realistically accomplish the net-zero decarbonization goal.

For this configuration the SOFC fulfills 60% of the electric demand, relying on 59% of green H_2 and 41% of grey H_2 during its operation. The

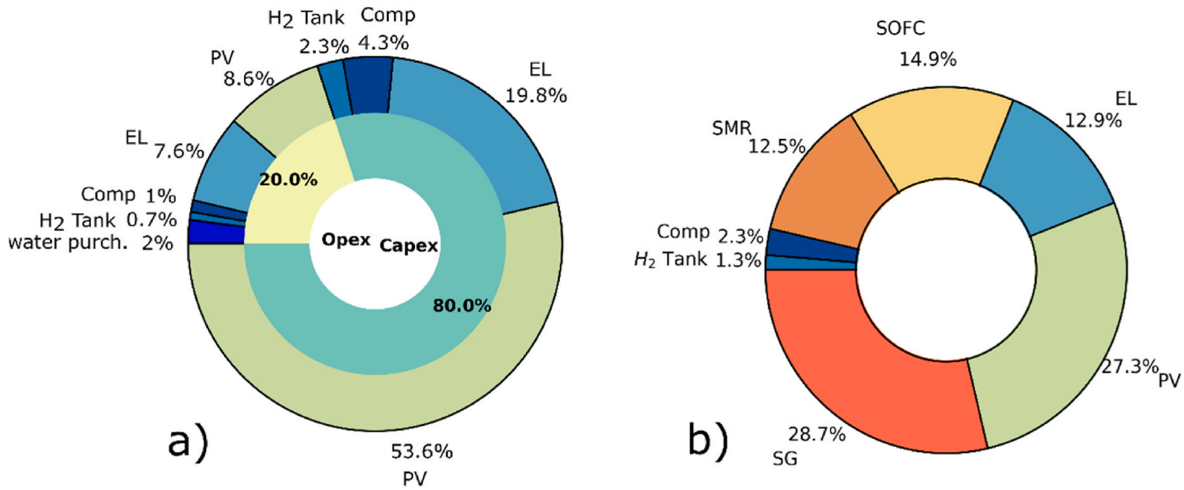

Fig. 14. LCOH (a) and NPC (b) percentage contributions in the optimal S2 configuration.

Table 7
LCOH and NPC numerical contributions in the optimal S2 configuration.

LCOH contribution	CAPEX [€/kg]	OPEX [€/kg]
PV	3.12	0.50
EL	1.15	0.44
Comp	0.25	0.06
H_2 Tank	0.13	0.04
Water purchased	–	0.12
Electricity sold	–	−0.55
	Without revenues [€/kg]	**With revenues [€/kg]**
Total	5.81	5.26
NPC contribution	**NPC [M€]**	
PV	50.1	
EL	23.8	
Comp	4.3	
H_2 Tank	2.4	
SMR	23.1	
SG	52.7	
SOFC	27.4	
Electricity sold	−7.6	
	Without revenues [M€]	**With revenues [M€]**
Total	183.8	176.2

PtH plant successfully produces 900 tons of green H_2. The thermal load is primarily met by the SG since the SOFC only covers 15% of it. Consequently, only a 25% reduction in CO_2 emissions is achieved compared to the GT scenario. The PV system fulfills nearly 40% of the remaining electric load, equivalent to 17.65 GWh (24% of the total PV production) allowing the plant to be almost totally independent from the electricity grid. The electrolyzer operation uses 46.21 GWh (63% of PV production), while the compressor operation consumes 1.82 GWh (2.5% of PV production). Additionally, a surplus of 7.64 GWh (10% of PV production) is fed back to the grid, resulting in a LCOH of 5.81€/kg (dropping to 5.26€/kg when considering electricity sold revenues).

Fig. 14 and Table 7 illustrate LCOH and NPCs percentage contributions in the identified S2 optimal configuration. It is evident how the PV impact on LCOH is predominant, exceeding 50% of the total (3.62 €/kg). However, taking into account that 24% of PV production is used to cover the electric load, a correspondent reduction of PV impact on LCOH calculation should be considered. This adjustment lowers its impact from 3.62 €/kg to 2.75 €/kg, resulting in a total LCOH of 4.95 €/kg (dropping to 4.4 €/kg when considering electricity sold revenues).

Regarding NPC contributions, not only PV but also SG and SMR have a significant impact. In fact, SG accounts for nearly 30% of the total NPCs, primarily due to the inclusion of NG purchase costs in its contribution. The revenues generated from electricity sales lowers the NPCs of approximately 4% from 183.8 M€ to 176.2 M€.

This study presents significant findings on decarbonization strategies for energy-intensive industries, providing a comprehensive examination of the applicability and potential of SOFC–CHP plants fuelled with hydrogen.

The research highlights the effectiveness of SOFCs in CHP applications while addressing challenges in integrating SOFCs with HRSGs to produce pressurized saturated steam, a critical thermal requirement in many energy-intensive sectors. This integration is found to be less efficient compared to gas turbines, due to the lower mass flow rates and higher vapor content present in SOFC exhaust. This disparity indicates that, for units of equivalent size, SOFCs not only yield lower flow rates but also fail to convert all latent heat from vapor at near-atmospheric pressure into pressurized saturated steam. This suggests that SOFCs are more suitable for industries with greater electrical demand than thermal load.

Regarding the PV-based green hydrogen production system, the study identifies an optimal PV-to-electrolyzer ratio of 2 to minimize LCOH, with a storage tank sized for daily capacity. However, to attain grid independence and meet fluctuating thermal and electric demands, supplementary components such as SMR for grey hydrogen production and SG for saturated steam generation are necessary.

3.3. Sensitivity analysis

Given the substantial impact of NG purchase and electricity sold prices on key economic indicators, a sensitivity analysis is carried out to further investigate their impact on the optimal configuration identified.

The optimal configuration of the plant prompts an in-depth exploration of the trends of LCOH and NPCs concerning key economic parameters that significantly influence these financial outcomes. In fact, in an era marked by economic uncertainties and geopolitical crises, the pivotal significance of conducting sensitivity analyses that account for substantial fluctuations in gas and electricity prices becomes increasingly important. Specifically, the analysis focuses on the variations of NG purchase price and electricity sold price. Given the plant's near-complete independence from the electricity grid, the electricity purchase price has not been taken into account.

The range for the electricity sold price spans from zero (no revenues scenario) to 200 €/MWh. This upper limit is derived from the maximum monthly price obtained by averaging values from the years 2020–2023, excluding 2022 due to the Ukraine war (GSE, 2023). Simultaneously, the NG purchase price is varied from zero (indicating no additional costs related to SMR and SG) to 100 €/MWh, a value recorded in Italy during

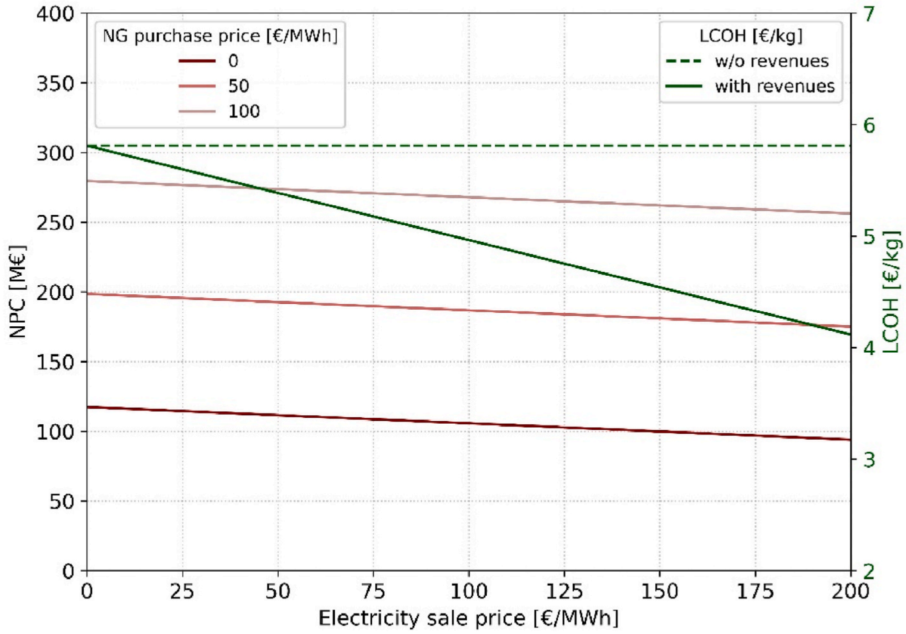

Fig. 15. LCOH (with and w/o revenues) and NPC (with revenues) in the optimal configuration as a function of the electricity sale price for three different NG purchase prices.

the first half of 2023 (Eurostat, 2023).

Fig. 15 reveals that the electricity sold price significantly influences LCOH calculation, leading to a linear decrease from 5.18 €/kg in the scenario with no revenues to 4.2 €/kg. In contrast, the impact on NPCs is less pronounced, given the involvement of all plant components (not only PtH ones). Although there is a marginal linear decline in NPCs as the electricity sold price increases, the NG purchase price is the predominant factor influencing the outcomes. For scenarios where electricity is not sold, increasing the NG purchase price from zero to 100 €/MWh, the NPCs vary substantially from 117.5 M€ to 279.6 M€ (138% increase), underlining how persistent is the dependence on the gas grid even in the identified optimal techno-economic configuration.

4. Conclusions

This research addresses the critical need for sustainable solutions to decarbonize energy-intensive industries. The primary objectives were to assess the techno-economic feasibility and environmental impact of replacing traditional gas turbine with a Solid Oxide Fuel Cell (SOFC) cogeneration system powered by on-site produced renewable hydrogen. Detailed models were developed for both the electrolyzer and the SOFC to accurately capture hourly system behavior under both nominal and partial load conditions. Additionally, the coupling of SOFC output mass flow rates with the heat recovery steam generator for producing pressurized saturated steam was modelled. The study utilized real data from the pulp and paper industry to compare three cogeneration alternatives: the conventional natural gas-powered gas turbine (current configuration), an SOFC using grey hydrogen from steam methane reforming, and a novel configuration powered by an SOFC using a mix of grey and green hydrogen produced via a PV-based electrolyzer system.

Key findings include.

- Integrating SOFC with heat recovery steam generator is less efficient compared to the gas turbine scenario due to lower mass flow rates and higher vapor content in SOFC exhaust gases. Consequently, SOFC produce 75% less pressurized saturated steam compared to a gas turbine of equivalent size.
- Using SOFCs fuelled only by grey hydrogen increases CO_2 emissions by 32% compared to the gas turbine configuration. This is due to the high natural gas consumption required for steam methane reforming, despite the higher electrical efficiency of the SOFC.
- The third studied configuration identified an optimal PV-to-electrolyzer ratio of 2 for the hydrogen production plant, achieving a LCOH of 5.81 €/kg, which is reduced to 4.4 €/kg when accounting for electricity sales and for the fact that 24% of PV production is used to cover the electric load. This setup achieved near-complete electricity grid independence and reduced CO_2 emissions by 25% compared to the gas turbine configuration. However, complete decarbonization remains unfeasible due to the need for a larger auxiliary steam generator.
- Sensitivity analysis shows electricity sale prices significantly impact LCOH, ranging from 5.18 €/kg to 4.2 €/kg with prices from 0 (excluding revenues) to 200 €/MWh. Natural gas prices also heavily influence net presents costs, increasing them from 200M€ to 280M€ as prices rise from 50 to 100 €/MWh due to reliance on the gas grid for steam reforming and generation.

While this analysis is specific to the pulp and paper industry, the model is replicable for various energy-intensive sectors. The requirement for a larger supplementary steam generator and the less efficient coupling with heat recovery steam generator imply that achieving complete decarbonization using SOFC cogeneration systems may be more favorable in industries where electrical demand surpasses thermal load. Future research should focus on advancing SOFC technology to enhance thermal efficiency and reduce supplementary steam generator reliance, exploring the scalability of the proposed system across different industries, and evaluating the long-term economic impacts of fluctuating renewable energy prices on the feasibility of hydrogen-based cogeneration systems.

CRediT authorship contribution statement

A. Ademollo: Writing – original draft, Validation, Software, Methodology, Investigation, Formal analysis, Data curation, Conceptualization. **A. Mati:** Writing – original draft, Validation, Software, Methodology, Investigation, Conceptualization. **M. Pagliai:** Writing – review & editing, Validation, Conceptualization. **C. Carcasci:** Writing – review & editing, Supervision.

Declaration of competing interest

The authors declare that they have no known competing financial interests or personal relationships that could have appeared to influence the work reported in this paper.

Data availability

Data will be made available on request.

Acknowledgements

This paper is written based on the cooperation between the "Dipartimento di Ingegneria Industriale, Università degli studi di Firenze, Italy" and "Dipartimento di Chimica 'Ugo Schiff', Università degli Studi di Firenze. This research did not receive any specific grant from funding agencies in the public, commercial, or not-for-profit sectors.

Nomenclature

Symbols

A	Area [m^2]
ASR	Area Specific Resistance [Ωcm^2]
CO_2	Carbon Dioxide [-]
c_p	Specific Heat constant [kJ/kg K]
D	Diffusivity [m^2/s]
E_0	Open circuit potential [V]
F	Faraday's constant [C/mol]
ΔG	Gibbs Free Energy [kJ/mol]
H_2O	Water [-]
H_2	Hydrogen [-]
HHV	Higher Heating value [kJ/mol]
i	Current density [A/cm^2]
i_0	Exchange current density [A/cm^2]
I	Current [A]
I_0	Total investment [€]
J_0	Activation Energy [kJ/mol]
k	Specific Constant [K/Ωm]
LHV	Lower Heating Value [kJ/kg]
M	Molar Mass [g/mol]
$\dot{m}$	Mass Flow Rate [kg/s]
N	Number of cells [-]
O_2	Oxygen [-]
Pr	Pressure [Pa]
P	Power [kW]
Q	Heat [kW]
R	Universal Gas Constant [J/mol K]
R^2	Coefficient of determination [-]
Δs_0	Entropy of formation [J/mol K]
ΔS	Molar Formation entropy [J/mol K]
t	Thickness [m]
T	Temperature [K]
T_0	Standard Temperature [K]
ΔT	Temperature difference [K]
V	Voltage [V]
ΔV	Voltage Losses [V]
x	Molar Fraction [-]
z	Molar Flow Rate [mol/s]

Greek Symbols

α	Transfer Coefficient [-]
η	Efficiency [-]
λ	Stoichiometric Coefficient [-]
σ	Conductivity [S/m]

Subscripts

act	Activation
air	Air
c	Cathode
cell	Cell
des	Design
eff	Effective

elec	Electrolyte
el	Electric
el_load	Electric load
g	gaseous
in	Inlet
min	Minimum
max	Maximum
nom	Nominal
out	Outlet
pp	Pinch point
prod	Produced
ref	reference
req	Required
st	Steam
stack	Stack
sub	Subcooling
sur	Surplus
th	Thermal
th_load	Thermal load
y	Year

Acronyms

CAPEX	Capital Expenditure
CF	Capacity Factor
CHP	Combined Heat and Power
EL	Electrolyzer
ESMS	Energy System Modular Solver
GT	Gas Turbine
HRSG	Heat Recovery Steam Generator
LCOH	Levelized Cost of Hydrogen
MCFC	Molten Carbonate Fuel Cells
MESS	Multi-Energy System Simulator
NG	Natural Gas
NPC	Net Present Cost
O&M	Operation & Maintenance
OPEX	Operational Expenditure
PEM	Proton Exchange Membrane
PPA	Power Purchase Agreement
PtH	Power to Hydrogen
PV	Photovoltaic
PVGIS	Photovoltaic Geographical Information System
rSOC	Reversible Solid Oxide Cell
SG	Steam Generator
SOEC	Solid Oxide Electrolysis Cell
SOFC	Solid Oxide Fuel Cell
SMR	Steam Methane Reformer
SOC	State of Charge

References

Abdin, Z., Mérida, W., 2019. Hybrid energy systems for off-grid power supply and hydrogen production based on renewable energy: a techno-economic analysis. Energy Convers. Manag. 196, 1068–1079. https://doi.org/10.1016/J.ENCONMAN.2019.06.068.

Ademollo, A., Ilo, A., Carcasci, C., 2023. End-use sector coupling to turn customer plants into prosumers of electricity and gas. In: 27th International Conference on Electricity Distribution (CIRED), pp. 357–361. https://doi.org/10.1049/ICP.2023.0308.

Ahmadi, R., Pourfatemi, S.M., Ghaffari, S., 2017. Exergoeconomic optimization of hybrid system of GT, SOFC and MED implementing genetic algorithm. Desalination 411, 76–88. https://doi.org/10.1016/J.DESAL.2017.02.013.

Arera: Dati e statistiche, 2023 [WWW Document]. https://www.arera.it/dati-e-statistiche?ambito=33&keyword=&settore=2&orderby=. accessed 1.21.24.

Arera: Prezzi e tariffe, 2023 [WWW Document]. https://www.arera.it/area-operatori/prezzi-e-tariffe. accessed 1.21.24.

Arsalis, A., 2019. A comprehensive review of fuel cell-based micro-combined-heat-and-power systems. Renew. Sustain. Energy Rev. 105, 391–414. https://doi.org/10.1016/J.RSER.2019.02.013.

Bhandari, R., Shah, R.R., 2021. Hydrogen as energy carrier: techno-economic assessment of decentralized hydrogen production in Germany. Renew. Energy 177, 915–931. https://doi.org/10.1016/J.RENENE.2021.05.149.

Bossel, U., 2012. Rapid startup SOFC modules. Energy Proc. 28, 48–56. https://doi.org/10.1016/j.egypro.2012.08.039.

Bottecchia, L., Lubello, P., Zambelli, P., Carcasci, C., Kranzl, L., 2021. The potential of simulating energy systems: the multi energy systems simulator model. Energies 14, 5724. https://doi.org/10.3390/EN14185724, 2021.

Burton, N.A., Padilla, R.V., Rose, A., Habibullah, H., 2021. Increasing the efficiency of hydrogen production from solar powered water electrolysis. Renew. Sustain. Energy Rev. 135, 110255 https://doi.org/10.1016/J.RSER.2020.110255.

Carcasci, C., Facchini, B., 1996. A numerical method for power plant simulations. J. Energy Resour. Technol. 118, 36–43. https://doi.org/10.1115/1.2792691.

Cinti, G., Bidini, G., Hemmes, K., 2019. Comparison of the solid oxide fuel cell system for micro CHP using natural gas with a system using a mixture of natural gas and hydrogen. Appl. Energy 238, 69–77. https://doi.org/10.1016/J.APENERGY.2019.01.039.

Cigolotti, V., Genovese, M., Fragiacomo, P., 2021. Comprehensive review on fuel cell technology for stationary applications as sustainable and efficient poly-generation energy systems. Energies 14, 4963. https://doi.org/10.3390/EN14164963, 2021.

DOE US, 2023. Land-Based Wind Market Report, 2023 Edition.

Ding, K., Li, A., Lv, J., Gu, F., 2023. Decarbonizing ceramic industry: technological routes and cost assessment. J. Clean. Prod. 419, 138278 https://doi.org/10.1016/J.JCLEPRO.2023.138278.

Dunkelberg, H., Wagner, J., Hannen, C., Schlüter, B.A., Phan, L., Hesselbach, J., Lin, C.X., 2018. Optimization of the energy supply in the plastics industry to reduce the primary energy demand. J. Clean. Prod. 192, 790–800. https://doi.org/10.1016/J.JCLEPRO.2018.04.254.

European Commission, 2023. Photovoltaic Geographical Information System (PVGIS) - European Commission [WWW Document]. URL. https://joint-research-centre.ec.europa.eu/photovoltaic-geographical-information-system-pvgis_en. accessed 1.21.24.

European Commission, 2022. REPowerEU [WWW Document]. URL. https://commission.europa.eu/strategy-and-policy/priorities-2019-2024/european-green-deal/repowereu-affordable-secure-and-sustainable-energy-europe_it. accessed 2.7.24.

European Commission, 2019. The European Green Deal [WWW Document]. URL. https://eur-lex.europa.eu/legal-content/EN/TXT/?uri=COM%3A2019%3A640%3AFIN. accessed 10.17.22.

Eurostat, 2023. File:F5Natural gas prices for non-household consumers. png - Statistics Explained [WWW Document]. URL. https://ec.europa.eu/eurostat/statistics-explained/index.php?title=File:F5Natural_gas_prices_for_non-household_consumers.png#file. accessed 1.22.24.

Fan, J.L., Yu, P., Li, K., Xu, M., Zhang, X., 2022. A levelized cost of hydrogen (LCOH) comparison of coal-to-hydrogen with CCS and water electrolysis powered by renewable energy in China. Energy 242, 123003. https://doi.org/10.1016/J.ENERGY.2021.123003.

Farfan, J., Fasihi, M., Breyer, C., 2019. Trends in the global cement industry and opportunities for long-term sustainable CCU potential for Power-to-X. J. Clean. Prod. 217, 821–835. https://doi.org/10.1016/J.JCLEPRO.2019.01.226.

Gallardo, F.I., Monforti Ferrario, A., Lamagna, M., Bocci, E., Astiaso Garcia, D., Baeza-Jeria, T.E., 2021. A Techno-Economic Analysis of solar hydrogen production by electrolysis in the north of Chile and the case of exportation from Atacama Desert to Japan. Int. J. Hydrogen Energy 46, 13709–13728. https://doi.org/10.1016/J.IJHYDENE.2020.07.050.

GenCell, 2023. Hydrogen & Ammonia Fuel Cell Power Solutions | GenCell [WWW Document]. URL. https://www.gencellenergy.com/. accessed 1.21.24).

Genovese, M., Schlüter, A., Scionti, E., Piraino, F., Corigliano, O., Fragiacomo, P., 2023. Power-to-hydrogen and hydrogen-to-X energy systems for the industry of the future in Europe. Int. J. Hydrogen Energy 48, 16545–16568. https://doi.org/10.1016/J.IJHYDENE.2023.01.194.

Global Efficiency Intelligence, 2023. Pulp and Paper Industry — Global Efficiency Intelligence [WWW Document]. URL. https://www.globalefficiencyintel.com/pulp-and-paper-industry. accessed 1.11.23.

Gorre, J., Ruoss, F., Karjunen, H., Schaffert, J., Tynjälä, T., 2020. Cost benefits of optimizing hydrogen storage and methanation capacities for Power-to-Gas plants in dynamic operation. Appl. Energy 257, 113967. https://doi.org/10.1016/J.APENERGY.2019.113967.

Griffin, P.W., Hammond, G.P., McKenna, R.C., 2021. Industrial energy use and decarbonisation in the glass sector: a UK perspective. Advances in Applied Energy 3, 100037. https://doi.org/10.1016/J.ADAPEN.2021.100037.

GSE, 2023. Documenti [WWW Document]. URL. https://www.gse.it/servizi-per-te/fotovoltaico/ritiro-dedicato/documenti. accessed 1.22.24.

He, F., Li, F., 2014. Hydrogen production from methane and solar energy – process evaluations and comparison studies. Int. J. Hydrogen Energy 39, 18092–18102. https://doi.org/10.1016/J.IJHYDENE.2014.05.089.

Hofrichter, A., Rank, D., Heberl, M., Sterner, M., 2023. Determination of the optimal power ratio between electrolysis and renewable energy to investigate the effects on the hydrogen production costs. Int. J. Hydrogen Energy 48, 1651–1663. https://doi.org/10.1016/J.IJHYDENE.2022.09.263.

IEA, 2023. Pulp and Paper – Analysis - IEA [WWW Document]. URL. https://www.iea.org/reports/pulp-and-paper. accessed 1.11.23.

INDEXBOX, 2023. Smr hydrogen plant cost - search - IndexBox [WWW Document]. URL. https://www.indexbox.io/search/smr-hydrogen-plant-cost/. accessed 1.21.24.

IRENA, 2021. Renewable Power Generation Costs in 2020 Executive Summary.

Jang, D., Kim, K., Kim, K.H., Kang, S., 2022. Techno-economic analysis and Monte Carlo simulation for green hydrogen production using offshore wind power plant. Energy Convers. Manag. 263, 115695 https://doi.org/10.1016/J.ENCONMAN.2022.115695.

Ju, H.K., Badwal, S., Giddey, S., 2018. A comprehensive review of carbon and hydrocarbon assisted water electrolysis for hydrogen production. Appl. Energy 231, 502–533. https://doi.org/10.1016/J.APENERGY.2018.09.125.

Katebah, M., Al-Rawashdeh, M., Linke, P., 2022. Analysis of hydrogen production costs in Steam-Methane Reforming considering integration with electrolysis and CO2 capture. Clean Eng Technol 10, 100552. https://doi.org/10.1016/J.CLET.2022.100552.

Lubello, P., Pasqui, M., Mati, A., Carcasci, C., 2022. Assessment of hydrogen based long term electrical energy storage in residential energy systems. Smart Energy 8, 100088. https://doi.org/10.1016/j.segy.2022.100088.

Lund, H., Thellufsen, J.Z., Østergaard, P.A., Sorknæs, P., Skov, I.R., Mathiesen, B.V., 2021. EnergyPLAN – advanced analysis of smart energy systems. Smart Energy 1, 100007. https://doi.org/10.1016/J.SEGY.2021.100007.

Marocco, P., Gandiglio, M., Audisio, D., Santarelli, M., 2023. Assessment of the role of hydrogen to produce high-temperature heat in the steel industry. J. Clean. Prod. 388, 135969 https://doi.org/10.1016/J.JCLEPRO.2023.135969.

Marocco, P., Gandiglio, M., Santarelli, M., 2024. Optimal design of PV-based grid-connected hydrogen production systems. J. Clean. Prod. 434, 140007 https://doi.org/10.1016/J.JCLEPRO.2023.140007.

Mati, A., Ademollo, A., Carcasci, C., 2023. Assessment of paper industry decarbonization potential via hydrogen in a multi-energy system scenario: a case study. Smart Energy 11, 100114. https://doi.org/10.1016/J.SEGY.2023.100114.

Mayer, T., Semmel, M., Guerrero Morales, M.A., Schmidt, K.M., Bauer, A., Wind, J., 2019. Techno-economic evaluation of hydrogen refueling stations with liquid or gaseous stored hydrogen. Int. J. Hydrogen Energy 44, 25809–25833. https://doi.org/10.1016/J.IJHYDENE.2019.08.051.

Meng, F., Rong, G., Zhao, R., Chen, B., Xu, X., Qiu, H., Cao, X., Zhao, L., 2024. Incorporating biochar into fuels system of iron and steel industry: carbon emission reduction potential and economic analysis. Appl. Energy 356, 122377. https://doi.org/10.1016/J.APENERGY.2023.122377.

Moran, C., Moylan, E., Reardon, J., Gunawan, T.A., Deane, P., Yousefian, S., Monaghan, R.F.D., 2023. A flexible techno-economic analysis tool for regional hydrogen hubs – a case study for Ireland. Int. J. Hydrogen Energy 48, 28649–28667. https://doi.org/10.1016/J.IJHYDENE.2023.04.100.

Mottaghizadeh, P., Jabbari, F., Brouwer, J., 2022. Integrated solid oxide fuel cell, solar PV, and battery storage system to achieve zero net energy residential nanogrid in California. Appl. Energy 323, 119577. https://doi.org/10.1016/J.APENERGY.2022.119577.

Nadir, M., Ghenaiet, A., Carcasci, C., 2016. Thermo-economic optimization of heat recovery steam generator for a range of gas turbine exhaust temperatures. Appl. Therm. Eng. 106, 811–826. https://doi.org/10.1016/J.APPLTHERMALENG.2016.06.035.

Nicita, A., Maggio, G., Andaloro, A.P.F., Squadrito, G., 2020. Green hydrogen as feedstock: financial analysis of a photovoltaic-powered electrolysis plant. Int. J. Hydrogen Energy 45, 11395–11408. https://doi.org/10.1016/J.IJHYDENE.2020.02.062.

Nikolaidis, P., Poullikkas, A., 2017. A comparative overview of hydrogen production processes. Renew. Sustain. Energy Rev. 67, 597–611. https://doi.org/10.1016/J.RSER.2016.09.044.

O'Hayre, R., 2016. Fuel Cell Fundamentals, third ed. 600.

Ozalp, N., Abedini, H., Abuseada, M., Davis, R., Rutten, J., Verschoren, J., Ophoff, C., Moens, D., 2022. An overview of direct carbon fuel cells and their promising potential on coupling with solar thermochemical carbon production. Renew. Sustain. Energy Rev. 162, 112427 https://doi.org/10.1016/J.RSER.2022.112427.

Pirkandi, J., Ghassemi, M., Hamedi, M.H., Mohammadi, R., 2012. Electrochemical and thermodynamic modeling of a CHP system using tubular solid oxide fuel cell (SOFC-CHP). J. Clean. Prod. 29–30, 151–162. https://doi.org/10.1016/J.JCLEPRO.2012.01.038.

Posdziech, O., Schwarze, K., Brabandt, J., 2019. Efficient hydrogen production for industry and electricity storage via high-temperature electrolysis. Int. J. Hydrogen Energy 44, 19089–19101. https://doi.org/10.1016/J.IJHYDENE.2018.05.169.

RedHawk Energy, 2023. Innovative Power Solutions | RedHawk Energy Systems. LLC [WWW Document]. URL. https://www.redhawkenergy.net/. accessed 1.21.24.

Salimbeni, A., Lombardi, G., Rizzo, A.M., Chiaramonti, D., 2023. Techno-Economic feasibility of integrating biomass slow pyrolysis in an EAF steelmaking site: a case study. Appl. Energy 339, 120991. https://doi.org/10.1016/J.APENERGY.2023.120991.

Shabbir, I., Mirzaeian, M., 2016. Feasibility analysis of different cogeneration systems for a paper mill to improve its energy efficiency. Int. J. Hydrogen Energy 41, 16535–16548. https://doi.org/10.1016/J.IJHYDENE.2016.05.215.

Shi, W., Zhu, J., Han, M., Sun, Z., Guo, Y., 2019. Operating limitation and degradation modeling of micro solid oxide fuel cell-combined heat and power system. Appl. Energy 252, 113444. https://doi.org/10.1016/J.APENERGY.2019.113444.

Shin, D., Kim, T., Kang, S., 2021. Design and performance analysis of a cascade solid oxide fuel cell system for high electrical efficiency. Appl. Therm. Eng. 195, 117214 https://doi.org/10.1016/J.APPLTHERMALENG.2021.117214.

Siemens Energy, 2023. SGT-100 [WWW Document]. URL. https://www.siemens-energy.com/global/en/home/products-services/product/sgt-100.html#Simple-cycle-power-generation-tab-4. accessed 1.25.24.

Singh, M., Zappa, D., Comini, E., 2021. Solid oxide fuel cell: decade of progress, future perspectives and challenges. Int. J. Hydrogen Energy 46, 27643–27674. https://doi.org/10.1016/J.IJHYDENE.2021.06.020.

Spirax Sarco, 2023. Water Tube Boilers | Spirax Sarco [WWW Document]. URL. https://www.spiraxsarco.com/learn-about-steam/the-boiler-house/water-tube-boilers. accessed 1.21.24.

Superchi, F., Mati, A., Carcasci, C., Bianchini, A., 2023. Techno-economic analysis of wind-powered green hydrogen production to facilitate the decarbonization of hard-to-abate sectors: a case study on steelmaking. Appl. Energy 342, 121198. https://doi.org/10.1016/J.APENERGY.2023.121198.

Tractebel, Engie, Hinicio, 2017. Study on Early Business Cases for H2 in Energy Storage and More Broadly Power to H2 Applications.

Trapani, D., Marocco, P., Gandiglio, M., Santarelli, M., 2023. Optimal design of a renewable power-to-hydrogen system for the decarbonization of a semiconductor industry. In: 36th International Conference on Efficiency, Cost, Optimization, Simulation and Environmental Impact of Energy Systems, ECOS 2023, pp. 2523–2531. https://doi.org/10.52202/069564-0227.

Tucker, M.C., 2010. Progress in metal-supported solid oxide fuel cells: a review. J. Power Sources 195, 4570–4582. https://doi.org/10.1016/j.jpowsour.2010.02.035.

Vialetto, G., Noro, M., Colbertaldo, P., Rokni, M., 2019. Enhancement of energy generation efficiency in industrial facilities by SOFC – SOEC systems with additional hydrogen production. Int. J. Hydrogen Energy 44, 9608–9620. https://doi.org/10.1016/J.IJHYDENE.2018.08.145.

Wang, F., Deng, S., Zhang, H., Wang, J., Zhao, J., Miao, H., Yuan, J., Yan, J., 2020. A comprehensive review on high-temperature fuel cells with carbon capture. Appl. Energy 275, 115342. https://doi.org/10.1016/J.APENERGY.2020.115342.

Wang, J., Yan, Z., Ma, S., Dai, Y., 2012. Thermodynamic analysis of an integrated power generation system driven by solid oxide fuel cell. Int. J. Hydrogen Energy 37, 2535–2545. https://doi.org/10.1016/J.IJHYDENE.2011.10.079.

Yates, J., Daiyan, R., Patterson, R., Egan, R., Amal, R., Ho-Baille, A., Chang, N.L., 2020. Techno-economic analysis of hydrogen electrolysis from off-grid stand-alone photovoltaics incorporating uncertainty analysis. Cell Rep Phys Sci 1, 100209. https://doi.org/10.1016/J.XCRP.2020.100209.

YongXing Boiler Group, 2023. The Smart Buyer's Guide to Industrial Steam Boiler Prices - Yongxing [WWW Document]. URL. https://www.yxboiler-factory.com/industrial-steam-boiler-prices/. accessed 1.21.24.

Zhao, X., Fu, L., Wang, X., Sun, T., Wang, J., Zhang, S., 2017. Flue gas recovery system for natural gas combined heat and power plant with distributed peak-shaving heat pumps. Appl. Therm. Eng. 111, 599–607. https://doi.org/10.1016/J.APPLTHERMALENG.2016.09.130.

Zhao, Y., Xue, H., Jiang, L., Jin, X., Fu, H., Xie, X., 2023. Proposal and assessment of a solid oxide fuel cell cogeneration system in order to produce high-temperature steam aiming at industrial applications. Appl. Therm. Eng. 221, 119882 https://doi.org/10.1016/J.APPLTHERMALENG.2022.119882.

Zhou, J., Wang, Z., Han, M., Sun, Z., Sun, K., 2022. Optimization of a 30 kW SOFC combined heat and power system with different cycles and hydrocarbon fuels. Int. J. Hydrogen Energy 47, 4109–4119. https://doi.org/10.1016/J.IJHYDENE.2021.11.049.